Bulletin of Mathematical Biology (2024) 86:25
https://doi.org/10.1007/s11538-023-01248-y

Society for Mathematical Biology

ORIGINAL ARTICLE


# Lyme Disease Models of Tick-Mouse Dynamics with Seasonal Variation in Births, Deaths, and Tick Feeding

**Kateryna Husar[1] · Dana C. Pittman[2] · Johnny Rajala[3] · Fahad Mostafa[4] · Linda J. S. Allen[4]**

Received: 10 May 2023 / Accepted: 19 December 2023


## Abstract

Lyme disease is the most common vector-borne disease in the United States impacting the Northeast and Midwest at the highest rates. Recently, it has become established in southeastern and south-central regions of Canada. In these regions, Lyme disease is caused by *Borrelia burgdorferi*, which is transmitted to humans by an infected *Ixodes scapularis* tick. Understanding the parasite-host interaction is critical as the white-footed mouse is one of the most competent reservoir for *B. burgdorferi*. The cycle of infection is driven by tick larvae feeding on infected mice that molt into infected nymphs and then transmit the disease to another susceptible host such as mice or humans. Lyme disease in humans is generally caused by the bite of an infected nymph. The main aim of this investigation is to study how diapause delays and demographic and seasonal variability in tick births, deaths, and feedings impact the infection dynamics of the tick-mouse cycle. We model tick-mouse dynamics with fixed diapause delays and more realistic Erlang distributed delays through delay and ordinary differential equations (ODEs). To account for demographic and seasonal variability, the ODEs are generalized to a continuous-time Markov chain (CTMC). The basic reproduction number and parameter sensitivity analysis are computed for the ODEs. The CTMC is used to investigate the probability of Lyme disease emergence when ticks and mice are introduced, a few of which are infected. The probability of disease emergence is highly dependent on the time and the infected species introduced. Infected mice introduced during the summer season result in the highest probability of disease emergence.

✉ Kateryna Husar
kat.husar@duke.edu

1 Department of Statistical Science, Duke University, Durham, NC 27705, USA

2 Department of Epidemiology and Biostatistics, Texas A&M University, College Station, TX 77843, USA

3 Department of Computer Science, University of Maryland, College Park, MD 20742, USA

4 Department of Mathematics and Statistics, Texas Tech University, Lubbock, TX 79409, USA

Published online: 31 January 2024

**Keywords** Differential equations · Lyme disease · Markov process · Ticks · Seasonality

**Mathematics Subject Classification** 92D30 · 60J28 · 34D20

## 1 Introduction

Lyme disease (also known as Lyme borreliosis) is the most common vector-borne disease in North America and Europe (Mead 2022). In the United States, the Centers for Disease Control and Prevention estimated the annual number of Lyme disease cases diagnosed and treated as 476,000 (based on 2010–2018 insurance claims data); over 90% are not reported (Kugeler et al. 2021). The majority of cases occur in the Northeast and Midwest regions of the United States, but Lyme disease is spreading into neighboring states and north into Canada (Chen et al. 2015; Public Health Agency of Canada (PHAC) 2023; Schwartz et al. 2017) Lyme disease is caused by the obligate parasite *Borrelia burgdorferi*, a slow growing spirochete bacterium (LoGiudice et al. 2003; Schwartz et al. 2017; Tilly et al. 2008). In the Northeast and Midwest regions, Lyme disease dynamics involve an interplay between the black-legged tick (*Ixodes scapularis*) and the white-footed mouse (*Peromyscus leucopus*). The primary reason *B. burgdorferi* remains in these populations is that infection does not impact the fitness of these species (Tilly et al. 2008). *Ixodes scapularis* nymphs are the disease vectors, with human spillover occurring most often by an infected nymph engorging on a person (Eisen et al. 2016; Schwartz et al. 2017; Tilly et al. 2008). In humans the infection may present with a “bull’s-eye" rash in the early stage progressing to arthritis and neurological issues as the body is extensively colonized (Tilly et al. 2008).

We focus on the Northeast region tick (*I. scapularis*) and seasonal timing associated with its life stages. *Ixodes scapularis* has four life stages with development taking place over two years, and seasonal variation playing a major role in the level of activity at each stage (Centers for Disease Control and Prevention (CDC) 2020; Eisen et al. 2016). The tick life cycle is described in Fig. 1 (Eisen et al. 2016). In our model, spring begins on May 1st, and each season lasts for 90 days. The seasonal timing simplifies the model and coincides with the beginning of nymph tick activity in Canada, as identified by Eisen et al. (2016) and Ogden et al. (2005). The tick life cycle begins in spring when adult female ticks lay eggs and then die. During the summer, eggs hatch into larvae, often feeding on *P. leucopus* because they are readily available on the forest floor. If the mouse is infected with *B. burgdorferi*, then the engorged larva will emerge in the autumn as an infected nymph. Through winter, nymphs enter diapause until the beginning of the second spring. Nymphal activity peaks between May and early July, with a broader questing range of possible hosts including both mice and humans. If infected nymphs engorge on susceptible mice, then these mice become infected, allowing for the persistence of Lyme disease. Another possible host of nymphs are humans that enter or live near endemically infected forests. The highest number of Lyme disease diagnoses in people occur during early July, two weeks after peak activity (nymph feeding), which provides further evidence that nymphs are the primary vector for transmission of infection to humans (Schwartz et al. 2017). In late summer through

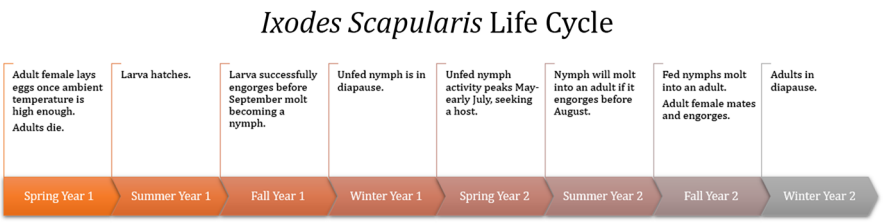


**Fig. 1** Two-year life cycle of *I. scapularis* (Eisen et al. 2016)

early fall, the nymphs molt into adults. Adult ticks are the most preferential in host selection, often selecting large mammals such as deer (Centers for Disease Control and Prevention (CDC) 2020; Cobbold et al. 2015). The high point for adult tick activity is the fall. This includes questing for a blood meal, and those successfully engorged will mate (Eisen et al. 2016). Then female ticks enter diapause over the winter and deposit the next generation of eggs in the spring (Eisen et al. 2016).

The white-footed mouse is the primary host reservoir because it is a competent host, unlike the deer. The white-footed mouse can be infected by a vector, maintain the infection, and pass it on to another feeding vector (Brunner and Ostfeld 2008; LoGiudice et al. 2003; Tilly et al. 2008). However, the deer is not a competent host as it is unable to be infected (Pearson et al. 2023). Also, deer are primarily fed on by adult ticks. The competency of the host *P. leucopus* and the vector *I. scapularis* drive the spread of Lyme disease in the absence of vertical transmission of *B. burgdorferi* in either the tick or the mouse (Eisen et al. 2016; Tilly et al. 2008). Therefore, our modeling focus is on the white-footed mouse as the primary host reservoir and on the seasonal variation in the tick cycle with three life stages, larva, nymph, and adult. Diapause is included in the tick stages.

Many Lyme disease models have captured the tick stages and their hosts through differential equations, difference equations, or in complex computational models, e.g. Caraco et al. (1998), Carrera-Pineyro et al. (2020), Cobbold et al. (2015), Gaff et al. (2020), Guo and Agusto (2022), Heffernan et al. (2014), Lou and Wu (2014), Lou and Wu (2017), Mount et al. (1997), Ostfeld et al. (2018). Several models include the effects of seasonality or developmental delays in tick and host dynamics as well as multiple host species and migrating birds that carry infected ticks, e.g. Cobbold et al. 2015, Fan et al. (2015), Heffernan et al. (2005), Lou et al. (2014), Mount et al. (1997), Ogden et al. (2007), Zhang and Wu (2019), Wang and Zhao (2017). Other models also include the effects of co-feeding, spatial spread, and control of ticks, e.g. Caraco et al. 2002, Fulk et al. (2022), Guo and Agusto (2022), Nah and Wu (2021), Wu and Zhang (2020), Zhang et al. (2021), Zhang and Zhao (2013). Each of these models provides different perspectives and new insights on ticks, hosts, and Lyme disease. For example, a discrete-time computational model, LYMESIM, originally developed by Mount et al. (1997) and updated by Gaff et al. (2020) is based on local and regional temperature and precipitation data and can be used as a public health tool to monitor the effectiveness of tick control measures. Many recent modeling approaches on tick-borne diseases that include co-feeding and developmental and behavioral delays are summarized in the book by Wu and Zhang (2020). The delay differential equations

(DDEs) for the Lyme disease model by Wang and Zhao (2017) motivates some of our research, but analysis of the DDE model is not the focus of this research. Our new modeling approach combines the tick two-year seasonal cycle with diapause delays in a stochastic, continuous-time Markov chain (CTMC). Our primary goal is to understand how demographic and seasonal variations affect disease emergence.

We formulate several deterministic models with increasing complexity to illustrate important model features in the tick-mouse cycle, culminating in an ODE framework that can be generalized to a CTMC model with demographic and environmental variability. First, we formulate a basic ODE model that illustrates the tick stages and feeding rates. Feeding results in the required blood meal for ticks to transition to the next stage and can also result in infection when either the ticks or the mice are infected. Second, we include fixed delays between the tick stages which leads to a system of DDEs. The delays in the DDEs mimic the instars experienced by ticks when they are inactive. Next, the fixed delays in the DDE model are extended to a more realistic Erlang-distributed delay through an ODE model with $n$ latent stages. The $n$ latent-stage ODE model is generalized to a stochastic CTMC model. Seasonal time-dependent parameters for birth and death of ticks and death in mice as well as larvae, nymph, and adult feeding rates are assumed that align with the two-year tick life cycle. Estimates for some of the models' parameters are obtained from data on field studies and laboratory observations in Ontario, Canada which have been published in the literature (Chen et al. 2015; Lindsay et al. 1995; Ogden et al. 2005; Schwartz et al. 2017).

The models are investigated analytically and numerically. We calculate and discuss the relevance of the basic reproduction number, $\mathcal{R}_0$, for the ODE and DDE models in a constant environment and numerically compute $\mathcal{R}_0$ for the ODE model in a seasonal environment. We also determine the numerical sensitivity of $\mathcal{R}_0$, the prevalence of infected nymphs and mice, and the density of infected nymphs to changes in the model parameters. Numerical simulations are used to compare the endemic dynamics of the DDE and ODE model and the initial behavior of the ODE and CTMC models.

As Lyme disease is spreading north to Canada and to other parts of the United States where the disease is not endemic (Eisen et al. 2016; Public Health Agency of Canada (PHAC) 2023; Ogden et al. 2008), it is important to investigate the potential for invasion of Lyme disease into new areas. Tick and mouse demographics and seasonal variability impact the probability and timing of invasion. Therefore, as the CTMC model with integer-valued random variables accounts for small numbers of ticks or mice, it is used to calculate the probabilities of disease extinction and consequently, the probabilities of disease emergence. These probabilities depend on the number of infected ticks and the season in which they are introduced.

## 2 Mathematical Models

First we discuss a basic ODE tick-mouse model and summarize some of the model assumptions regarding tick feeding and transmission rates. Then we discuss a DDE model for the modeling of time delays in the tick cycle. The DDE model incorporates three fixed time delays for molting from larva to nymph and nymph to adult and for

reproduction in the adult stage. The fixed delays in the DDE are generalized to an Erlang distribution which results in an ODE model with $n$ latent stages. As $n \to \infty$, the Erlang density approaches that of a fixed delay. The assumptions in the $n$-stage ODE model lead to the formulation of the CTMC model.

### 2.1 ODE Tick-Mouse Model

Let $L$, $N^S$, $N^I$, $A$, $M^S$, and $M^I$ be the population densities (per km$^2$) of tick larvae, susceptible tick nymphs, infected tick nymphs, adult ticks, susceptible mice, and infected mice, respectively. Let $M = M^S + M^I$ and $N = N^S + N^I$. The list of other variables and parameters along with their biological descriptions are summarized in Table 1. We assume there is a maximum number of larvae, nymphs, or adult ticks can feed on a mouse or deer. In particular, a type II functional response in tick density/host is assumed by Cobbold et al. (2015), where the feeding rate for larvae on mice takes the form $F_L M L/(a_L + L)$, where $a_L$ is the half maximum carrying capacity of larvae per km$^2$. In our model, we assume that the saturation of ticks on hosts is related to host density, and we replace $a_L$ with $m_L M$, where $m_L$ is half of the maximum number of ticks per mouse as in Maliyoni et al. (2017). Thus, the feeding rate for larvae on mice is

$$F_L M \frac{L}{m_L M + L}.$$

Similar forms are assumed for the feeding rates of nymphs on mice and adult ticks on deer,

$$F_N M \frac{N^i}{m_N M + N},\ i = S, I, \quad F_A D \frac{A}{m_A D + A},$$

respectively. Another assumption made by Cobbold et al. (2015) is that successful larval feeding on an infected mouse results in transmission of the infection with probability one, i.e., $\beta_L = 1$. Here, we distinguish between feeding and transmission and for model generality, we retain the transmission probability $\beta_L$ separately from the feeding rate $F_L$.

Adult tick infection does not result in vertical transmission to the eggs. That is, there is no transovarial transmission of *B. burgdorferi* in *I. scapularis* (Rollend et al. 2013); a larval tick is always susceptible before feeding on a mouse. If a larva feeds on a susceptible mouse, it stays susceptible and molts into a susceptible nymph. But if the mouse is infected, the larva becomes infected with probability $\beta_L$ and molts into an infected nymph. A nymph then feeds on a mouse to become an adult. If an infected nymph feeds on a susceptible mouse, it may transmit *B. burgdorferi* to the mouse with probability $\beta_M$. An adult tick has its final feeding in fall, after which it may survive the winter and lay eggs that hatch to become larvae, completing the cycle. The compartmental diagram and parameters of the basic ODE model are described in Fig. 2 and Table 1, respectively.

**Table 1** ODE and DDE parameters and their biological meaning

| Parameter | Description | Units * | Value † | References |
|---|---|---|---|---|
| $b_T$ | Number of eggs per adult that survive to larvae | larva · adult$^{-1}$ | – | NA |
| $F_L$ | Larval feeding rate per mouse | larva · (day · mouse)$^{-1}$ | – | NA |
| $F_N$ | Nymphal feeding rate per mouse | nymph · (day · mouse)$^{-1}$ | – | NA |
| $F_A$ | Adult feeding rate per deer | adult · (day · deer)$^{-1}$ | – | NA |
| $e_L$ | Larval survival during diapause | – | – | NA |
| $e_N$ | Nymphal survival during diapause | – | – | NA |
| $e_A$ | Adult tick survival during diapause | – | – | NA |
| $\mu_L$ | Larval death rate | day$^{-1}$ | – | NA |
| $\mu_N$ | Nymphal death rate | day$^{-1}$ | – | NA |
| $\mu_A$ | Adult tick death rate | day$^{-1}$ | – | NA |
| $\tau_L$ | Average duration after larval feeding to molt to nymph | day | 21.5 | Apanaskevich and Oliver (2013) |
| $\tau_N$ | Average duration after nymph feeding to molt to adult | day | 26 | Apanaskevich and Oliver (2013) |
| $\tau_A$ | Average duration after adult feeding to lay eggs | day | 180 | Eisen et al. (2016) |
| $b_M$ | Mouse birth rate | day$^{-1}$ | – | NA |
| $d$ | Mouse density-independent death rate | day$^{-1}$ | – | NA |
| $d_{\min}$ | Mouse baseline death rate | day$^{-1}$ | 0.012 | Ogden et al. (2007) |
| $\Delta d$ | Mouse change in winter death rate | day$^{-1}$ | 0.004 | Ogden et al. (2007) |
| $d_M$ | Mouse density-dependent death rate | day$^{-1}$ | – | NA |
| $\beta_L$ | Probability of transmission from infected mouse to larva | – | 1 | Cobbold et al. (2015) |
| $\beta_M$ | Competency of infected nymph to pass infection to mouse | mouse · (infected nymph)$^{-1}$ | 0.75 | NA |

**Table 1** continued

| Parameter | Description | Units * | Value † | References |
|---|---|---|---|---|
| $m_L$ | Average number of larvae per mouse | larva·(mouse)$^{-1}$ | 27.8[a] | LoGiudice et al. (2003) |
| $m_N$ | Average number of nymphs per mouse | nymph·(mouse)$^{-1}$ | 2.5[a] | Ogden et al. (2005) |
| $m_A$ | Average number of adult ticks per deer | adult·(deer)$^{-1}$ | 239[a] | LoGiudice et al. (2003) |
| $A_b$ | Maximum number of eggs per adult tick | eggs · (adult)$^{-1}$ | 2273.9035[b] | Lindsay et al. (1995) |
| $A_{l\,\max}$ | Maximum larval death rate | day$^{-1}$ | 0.006 | Ogden et al. (2007) |
| $A_{l\,\min}$ | Minimum larval death rate | day$^{-1}$ | 0.003 | Ogden et al. (2007) |
| $A_{n\,\max}$ | Maximum nymphal death rate | day$^{-1}$ | 0.006 | Ogden et al. (2007) |
| $A_{n\,\min}$ | Minimum nymphal death rate | day$^{-1}$ | 0.002 | Ogden et al. (2007) |
| $A_{a\,\max}$ | Maximum adult tick death rate | day$^{-1}$ | 0.006 | Ogden et al. (2007) |
| $A_{a\,\min}$ | Minimum adult tick death rate | day$^{-1}$ | 0.0001 | Ogden et al. (2007) |
| $b_M$ | Mouse litter size | mice · (day)$^{-1}$ | 0.01875[b] | Ogden et al. (2007) |
| $A_l$ | Maximum larval feeding rate (max $F_L$) | larva · (mouse · day)$^{-1}$ | 0.4876[b] | Cobbold et al. (2015) |
| $A_n$ | Maximum nymphal feeding rate (max $F_N$) | nymph · (mouse · day)$^{-1}$ | 0.0115[b] | Cobbold et al. (2015) |
| $A_a$ | Maximum adult tick feeding rate (max $F_A$) | adult · (deer · day)$^{-1}$ | 3.3997[b] | Cobbold et al. (2015) |
| $D$ | Deer population density | deer · (km$^2$)$^{-1}$ | 10 | Chen et al. (2015) |
| $K$ | Mouse scaled carrying capacity | mice · (km$^2$)$^{-1}$ | 150[b] | Vessey (1987) |

* Parameters with no units are marked with dash
† Non-constant parameters do not have constant values, thus are marked with dash
[a] Average body burden, assumed to be half of the maximum value
[b] Further calculations performed on the original value from reference (see Appendix B)

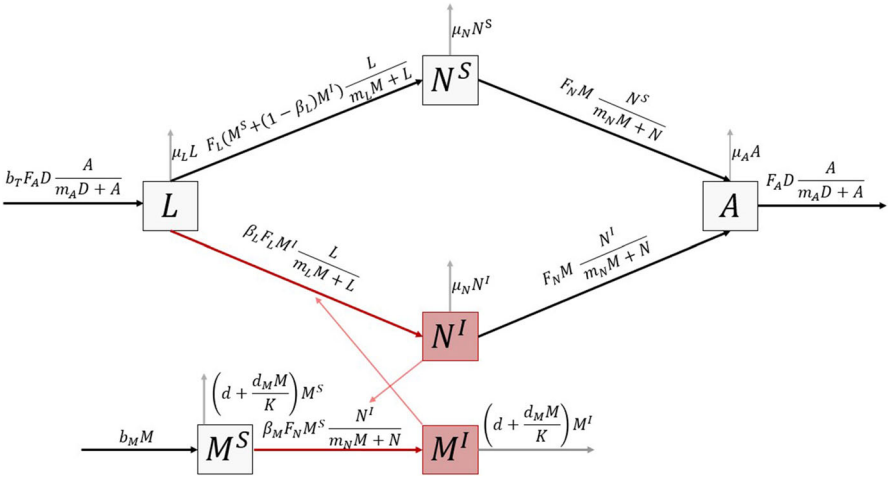


**Fig. 2** Compartmental diagram for the basic ODE tick-mouse model, $N = N^S + N^I$ and $M = M^S + M^I$

In the mouse dynamics, we apply a logistic-like form with density-dependent deaths, often assumed in deer or mouse populations that serve as reservoir hosts for Lyme and other diseases (Gaff and Gross 2007; Maliyoni et al. 2017; Sauvage et al. 2003; Wesley and Allen 2009). Mice become infected when infected nymphs feed on them. The differential equations for the tick and mouse dynamics are:

$$\text{Tick} \begin{cases} \dfrac{dL}{dt} &= b_T F_A D \dfrac{A}{m_A D + A} - F_L M \dfrac{L}{m_L M + L} - \mu_L L \\ \dfrac{dN^S}{dt} &= F_L \left(M^S + (1-\beta_L) M^I\right) \dfrac{L}{m_L M + L} - F_N M \dfrac{N^S}{m_N M + N} - \mu_N N^S \\ \dfrac{dN^I}{dt} &= \beta_L F_L M^I \dfrac{L}{m_L M + L} - F_N M \dfrac{N^I}{m_N M + N} - \mu_N N^I \\ \dfrac{dA}{dt} &= F_N M \dfrac{N}{m_N M + N} - F_A D \dfrac{A}{m_A D + A} - \mu_A A. \end{cases} \tag{1}$$

$$\text{Mouse} \begin{cases} \dfrac{dM^S}{dt} &= b_M M - M^S \left(d + d_M \dfrac{M}{K}\right) - \beta_M F_N M^S \dfrac{N^I}{m_N M + N} \\ \dfrac{dM^I}{dt} &= \beta_M F_N M^S \dfrac{N^I}{m_N M + N} - M^I \left(d + d_M \dfrac{M}{K}\right). \end{cases} \tag{2}$$

Next we include the diapause and reproduction delays in the tick population.

### 2.2 DDE Tick Model

The DDE model generalizes the ODE model from the previous section by including three time delays after feeding at each tick life stage, $L$, $N$, and $A$. The delays are denoted as $\tau_L$, $\tau_N$, and $\tau_A$, respectively. These delays are representative of instars experienced by ticks when they are inactive, following a blood meal. While the tick is at instar state, there is still the possibility of death. Thus, only a proportion of the fed ticks survive and either molt to the next stage (larvae and nymphs) or mate and reproduce eggs (adults) (Lindsay et al. 1995). The survival proportions of the three stages are denoted $e_L$, $e_N$, and $e_A$ in the DDE model. Specifically, the probability of survival at each stage can be calculated by integrating the differential equation that relates to deaths $\frac{dx}{dt} = -\mu_x(t)x$ (tick life stage $x = L, N, A$) over the time interval $[t - \tau_x, t]$. This results in the proportion of ticks in stage $x$ that survive:

$$e_x \equiv e_x(t - \tau_x, t) = \exp\left(-\int_{t-\tau_x}^{t} \mu_x(r)dr\right), \ x = L, N, A.$$

For a constant death rate $\mu_x$, the proportion simplifies to $e_x \equiv e^{-\mu_x \tau_x}$, $x = L, N, A$, i.e,

$$e_L = e^{-\mu_L \tau_L}, \quad e_N = e^{-\mu_N \tau_N}, \quad e_A = e^{-\mu_A \tau_A}. \tag{3}$$

Under these assumptions we obtain the following DDE tick model:

$$\text{Tick} \begin{cases} \dfrac{dL}{dt} &= b_T e_A(t-\tau_A,t) F_A(t-\tau_A) D \dfrac{A(t-\tau_A)}{m_A D + A(t-\tau_A)} - F_L M \dfrac{L}{m_L M + L} - \mu_L L \\ \dfrac{dN^S}{dt} &= e_L(t-\tau_L,t) F_L(t-\tau_L) \left[M^S(t-\tau_L) + (1-\beta_L) M^I(t-\tau_L)\right] \dfrac{L(t-\tau_L)}{m_L M(t-\tau_L) + L(t-\tau_L)} \\ &\quad - F_N M \dfrac{N^S}{m_N M + N} - \mu_N N^S \\ \dfrac{dN^I}{dt} &= e_L(t-\tau_L,t) \beta_L F_L(t-\tau_L) M^I(t-\tau_L) \dfrac{L(t-\tau_L)}{m_L M(t-\tau_L) + L(t-\tau_L)} \\ &\quad - F_N M \dfrac{N^I}{m_N M + N} - \mu_N N^I \\ \dfrac{dA}{dt} &= e_N(t-\tau_N,t) F_N(t-\tau_N) M(t-\tau_N) \dfrac{N(t-\tau_N)}{m_N M(t-\tau_N) + N(t-\tau_N)} \\ &\quad - F_A D \dfrac{A}{m_A D + A} - \mu_A A. \end{cases} \tag{4}$$

The parameters in the DDE model are the same as those in the ODE model (1) with the exception of the delays and the survival times, which are described in Table 1. All non-constant parameters and state variables are assumed to be evaluated at time $t$, unless specified otherwise, in which case they are evaluated before the instar period. DDE models for Lyme disease with various types of fixed delays in the tick stages have been studied by Fan et al. (2015) and Wang and Zhao (2017). Our model is more closely related to that of Wang and Zhao (2017). Their DDE model differs from our model in the assumptions regarding the birth and transmission functions, the seasonality in

births and biting rates, and the delays for feeding durations (Wang and Zhao 2017). Our delays represent diapause delays with seasonal births, deaths, and feeding rates leading to a two-year tick life cycle. We generalize the delays to Erlang distributions that lead to an ODE system with latent stages.

### 2.3 ODE Tick Model with Latent Stages

The fixed delays in the DDE tick model are generalized to an Erlang distribution by including additional stages within each life stage, larva, nymph, and adult. These additional stages are referred to as latent stages. Extending the ODE tick model to $n$ latent stages for each of the three delays changes the fixed delays with Dirac delta distributions to Erlang distributions with means $\tau_L$, $\tau_N$, and $\tau_A$, respectively (Appendix A). As the number $n$ of latent stages increases, the Erlang density approaches the Dirac delta function with impulse centered at the delay (Lloyd 2001). There are two advantages of this extension. First, the Erlang density is more realistic than the fixed delay and second, the model with latent stages can be easily generalized to a CTMC model with discrete events.

The delays are divided into $n$ latent stages each with average duration of $\tau_x/n$ or a departure rate of $n/\tau_x$, $x = L, N, A$. The general form of the $n$-stage ODE tick model is defined by Eqs. (5)–(10). The larval delay begins after a larva successfully feeds on a mouse and enters either stage $L_1^S$ or $L_1^I$, depending on whether the mouse is infected. The larva transitions through $n$ latent stages at rate $n/\tau_L$ (Eqs. (6)) until it becomes a susceptible or infected nymph, $N^S$ or $N^I$ (Eqs. (7)). This is followed by a second feeding on a mouse and a second delay where the susceptible or infected nymph passes through $n$ latent stages at rate $n/\tau_N$ (Eqs. (8)) until the nymph becomes an adult (Eq. (9)). After the adult tick feeds on a deer, the female mates and goes through diapause, represented by the $n$ stages, at a rate $n/\tau_A$ (Eqs. (9)) until eggs are laid. Female ticks die and eggs become larvae in the spring. We do not track infected adults, as they feed primarily on large mammals such as deer. Also, adult ticks on humans are easily detected and removed before the infection can be transmitted.

$$\text{Larvae}\ \left\{\ \frac{dL}{dt} = b_T \frac{n}{\tau_A} A_n - F_L M \frac{L}{m_L M + L} - \mu_L L \right. \tag{5}$$

$$\text{Larvae transition}\ \begin{cases} \dfrac{dL_1^S}{dt} = F_L(M^S + (1-\beta_L)M^I)\dfrac{L}{m_L M + L} - \dfrac{n}{\tau_L} L_1^S - \mu_L L_1^S \\ \dfrac{dL_1^I}{dt} = \beta_L F_L M^I \dfrac{L}{m_L M + L} - \dfrac{n}{\tau_L} L_1^I - \mu_L L_1^I \\ \dfrac{dL_k^j}{dt} = \dfrac{n}{\tau_L} L_{k-1}^j - \dfrac{n}{\tau_L} L_k^j - \mu_L L_k^j, \qquad k = 2, \ldots, n,\ j = S, I, \end{cases} \tag{6}$$

$$\text{Nymphs}\ \begin{cases} \dfrac{dN^S}{dt} = \dfrac{n}{\tau_L} L_n^S - F_N M \dfrac{N^S}{m_N M + N} - \mu_N N^S \\ \dfrac{dN^I}{dt} = \dfrac{n}{\tau_L} L_n^I - F_N M \dfrac{N^I}{m_N M + N} - \mu_N N^I, \quad N = N^S + N^I \end{cases} \tag{7}$$

$$\text{Nymph Transition} \begin{cases} \dfrac{dN_1^S}{dt} &= F_N M^S \dfrac{N^S}{m_N M + N} - \dfrac{n}{\tau_N} N_1^S - \mu_N N_1^S \\ \dfrac{dN_1^I}{dt} &= F_N \dfrac{N^S M^I + N^I M}{m_N M + N} - \dfrac{n}{\tau_N} N_1^I - \mu_N N_1^I \\ \dfrac{dN_k^j}{dt} &= \dfrac{n}{\tau_N} N_{k-1}^j - \dfrac{n}{\tau_N} N_k^j - \mu_N N_k^j, \qquad k = 2, \ldots, n, \ j = S, I. \end{cases} \tag{8}$$

$$\text{Adult} \left\{ \frac{dA}{dt} = \frac{n}{\tau_N} \left( N_n^S + N_n^I \right) - F_A D \frac{A}{m_A D + A} - \mu_A A \right. \tag{9}$$

$$\text{Adult Transition} \begin{cases} \dfrac{dA_1}{dt} &= F_A D \dfrac{A}{m_A D + A} - \dfrac{n}{\tau_A} A_1 - \mu_A A_1 \\ \dfrac{dA_k}{dt} &= \dfrac{n}{\tau_A} A_{k-1} - \dfrac{n}{\tau_A} A_k - \mu_A A_k, \qquad k = 2, \ldots, n. \end{cases} \tag{10}$$

The mouse model is the same as in Eq. (2); delays are not included in the mouse model.

### 2.4 Markov Chain Model

We now formulate a CTMC model based on the $n$-latent stage ODE model. In the CTMC model, time is continuous-valued, $t \in [0, \infty)$, and the random variables are discrete-valued, i.e.,

$$L_k^j, N_k^j, A_k, M^j \in \{0, 1, 2, \ldots\}, \quad j = I, S; \ k = 1, \ldots, n.$$

For simplicity, the same notation is used for the variables in the CTMC as in the ODE model. In general, stochastic epidemic models encapsulate the randomness in birth, death, and transmission, which is especially important when number of infected individuals is few. The term "Markov" in "CTMC" implies that the process has the *memoryless property*, meaning the future state is dictated by the present, independently of the past. Since the fixed delay DDE model relies on the values of the population at some past time, it cannot be directly related to the CTMC model. Therefore, the $n$ latent stage ODE model motivates the formulation of the CTMC model.

The CTMC model is defined by events that result in a change of either $+1$ or $-1$ in a random variable and the probability associated with each event. These probabilities are obtained from the rates in the ODE model by multiplying them by a small period of time $\Delta t$. We apply a Monte Carlo simulation instead of calculating the interevent time with the Gillespie algorithm (Gillespie 1977). Calculation of interevent time is more complex in a time-nonhomogeneous process than with constant parameters, and requires inversion of an integral equation at each change (Shakiba et al. 2021). Instead we apply a Monte Carlo method by incrementing time by a sufficiently small positive time step $\Delta t$, so that at most one event occurs each time step, and such that the sum of the probabilities in Table 2 is always less than unity. An event can be visualized as movement along an arrow between two compartments in the ODE compartmental diagram in Fig. 3. The list of all possible events and the transitions are summarized in Table 2. Details on specific functional forms for the parameters that include seasonal variation are described in the next section.

**Table 2** CTMC events and rates

| Event | Description | Transitions | Rate* |
|---|---|---|---|
| 1 | Larva birth | $L \to L+1$ | $b_T \frac{n}{\tau_A} A_n$ |
| 2 | Larva death | $L \to L-1$ | $\mu_L L$ |
| 3 | Larva feeds on susceptible mouse | $L \to L-1; L_1^S \to L_1^S+1$ | $F_L \left(M^S + (1-\beta_L) M^I\right) \frac{L}{m_L M+L}$ |
| 4 | Larva feeds on infected mouse | $L \to L-1; L_1^I \to L_1^I+1$ | $\beta_L F_L M^I \frac{L}{m_L M+L}$ |
| $4+k^{\mathrm{a}}$ | Susceptible larva transitions during delay | $L_k^S \to L_k^S-1; L_{k+1}^S \to L_{k+1}^S+1$ | $\frac{n}{\tau_L} L_k^S$ |
| $4+n-1+k^{\mathrm{a}}$ | Infected larva transitions during delay | $L_k^I \to L_k^I-1; L_{k+1}^I \to L_{k+1}^I+1$ | $\frac{n}{\tau_L} L_k^I$ |
| $4+2(n-1)+k^{\mathrm{b}}$ | Susceptible larva death during delay | $L_k^S \to L_k^S-1$ | $\mu_L L_k^S$ |
| $3n+2+k^{\mathrm{b}}$ | Infected larva death during delay | $L_k^I \to L_k^I-1$ | $\mu_L L_k^I$ |
| $4n+3$ | Susceptible larva transitions to susceptible nymph | $L_n^S \to L_n^S-1; N^S \to N^S+1$ | $\frac{n}{\tau_L} L_n^S$ |
| $4n+4$ | Infected larva transitions to infected nymph | $L_n^I \to L_n^I-1; N^I \to N^I+1$ | $\frac{n}{\tau_L} L_n^I$ |
| $4n+5$ | Susceptible nymph death | $N^S \to N^S-1$ | $\mu_N N^S$ |
| $4n+6$ | Infected nymph death | $N^I \to N^I-1$ | $\mu_N N^I$ |
| $4n+7$ | Susceptible nymph feeds on susceptible mouse | $N^S \to N^S-1; N_1^S \to N_1^S+1$ | $F_N M^S \frac{N^S}{m_N M+N}$ |
| $4n+8$ | Susceptible nymph feeds on infected mouse | $N^S \to N^S-1; N_1^I \to N_1^I+1$ | $F_N M^I \frac{N^S}{m_N M+N}$ |
| $4n+9$ | Infected nymph feeds on mouse | $N^I \to N^I-1; N_1^I \to N_1^I+1$ | $F_N M \frac{N^I}{m_N M+N}$ |
| $4n+9+k^{\mathrm{a}}$ | Susceptible nymph transitions during delay | $N_k^S \to N_k^S-1; N_{k+1}^S \to N_{k+1}^S+1$ | $\frac{n}{\tau_N} N_k^S$ |
| $5n+8+k^{\mathrm{a}}$ | Infected nymph transitions during delay | $N_k^I \to N_k^I-1; N_{k+1}^I \to N_{k+1}^I+1$ | $\frac{n}{\tau_N} N_k^I$ |
| $6n+7+k^{\mathrm{b}}$ | Susceptible nymph death during delay | $N_k^S \to N_k^S-1$ | $\mu_N N_k^S$ |

**Table 2** continued

| Event | Description | Transitions | Rate* |
|---|---|---|---|
| $7n+7+k$ [b] | Infected nymph death during delay | $N_k^I \to N_k^I - 1$ | $\mu_N N_k^I$ |
| $8n+8$ | Susceptible nymph transitions to adult | $N_n^S \to N_n^S - 1; A \to A+1$ | $\frac{n}{\tau_N} N_n^S$ |
| $8n+9$ | Infected nymph transitions to adult | $N_n^I \to N_n^I - 1; A \to A+1$ | $\frac{n}{\tau_N} N_n^I$ |
| $8n+10$ | Adult feeds on deer | $A \to A-1; A_1 \to A_1+1$ | $F_A D \frac{A}{m_A D+A}$ |
| $8n+11$ | Adult death | $A \to A-1$ | $\mu_A A$ |
| $8n+11+k$ [a] | Adult transition during delay | $A_k \to A_k - 1; A_{k+1} \to A_{k+1}+1$ | $\frac{n}{\tau_A} A_k$ |
| $9n+10+k$ [b] | Adult death during delay | $A_k \to A_k - 1$ | $\mu_A A_k$ |
| $10n+11$ | Adult death after reproduction | $A_n \to A_n - 1$ | $\frac{n}{\tau_A} A_n$ |
| $10n+12$ | Mouse birth | $M^S \to M^S + 1$ | $b_M M$ |
| $10n+13$ | Susceptible mouse death | $M^S \to M^S - 1$ | $M^S \left(d + d_M \frac{M}{K}\right)$ |
| $10n+14$ | Infected mouse death | $M^I \to M^I - 1$ | $M^I \left(d + d_M \frac{M}{K}\right)$ |
| $10n+15$ | Susceptible mouse infected from nymph feeding | $M^S \to M^S - 1; M^I \to M^I + 1$ | $\beta_M F_N M^S \frac{N^I}{m_N M+N}$ |

*Probability: rate $\cdot \Delta t + o(\Delta t)$ [a] $k = 1, \ldots, n-1$ [b] $k = 1, \ldots, n$

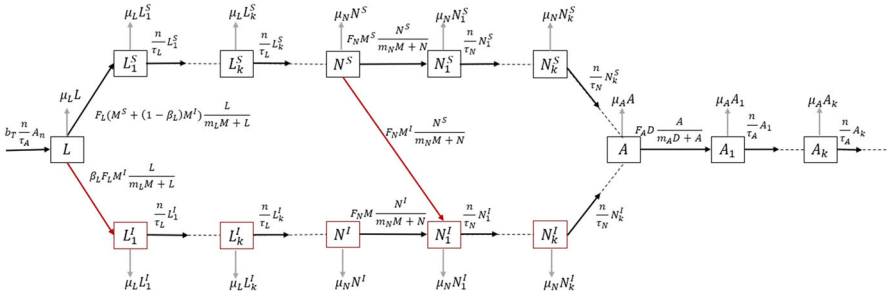


**Fig. 3** Compartmental diagram of tick life cycle for the ODE model with $n$ latent stages for each delay

## 3 Parameters

The effects of seasonality are included in the models through assumptions regarding the time-dependence of some of the parameters. In particular, we assume that the tick birth, death, and feeding rates are periodic to account for the change in tick populations throughout the year and the seasonality present in tick activity. These assumptions come from observations on tick behavior (Eisen et al. 2016). Estimates for the parameter values come from the literature pertaining to tick biology and Lyme disease ecology (Apanaskevich and Oliver 2013; Chen et al. 2015; Cobbold et al. 2015; Lindsay et al. 1995; Ogden et al. 2004, 2007; Vessey 1987). We applied trigonometric functions for ease in making annual periodic functions and a maximum function to ensure rates are nonnegative. When feasible, estimates from field data were used for the numerical value, but if data were unavailable, estimates from laboratory observations were used. To ensure all units were in agreement, all units were converted to days and to km$^2$.

The information regarding the values of the delays $\tau_L$ and $\tau_N$ is taken from Apanaskevich and Oliver (2013), a textbook on the biology of ticks. In our models, we used the average length of the delays. The average length of the delays experienced at each transitional stage is based on a laboratory experiment oriented at the development of ticks. According to Apanaskevich and Oliver (2013), the delay for larvae is 16–27 days, and the delay for nymphs is 18–34 days. Without the inclusion of $\tau_L$ and $\tau_N$, the model moves ticks between populations too rapidly. The $\tau_A$ term is associated with diapause (Eisen et al. 2016) and frequently observed in adults as a method for increasing the survival of eggs over the cold winter months. The value of $\tau_A$ is assumed to have an average 180 days (Apanaskevich and Oliver 2013). All death rates listed in Table 1 are from reference (Ogden et al. 2007), a mathematical modeling paper that collected field data from Ontario, Canada. The minimum and maximum death per day observed for each tick life stage is used as the amplitude bounds for the periodic functions. The idea for implementing a periodic death parameter came from references (Eisen et al. 2016; Lindsay et al. 1995; Ogden et al. 2007). An increase in the mouse death rate over the winter was observed in Ogden et al. (2007) due to limitations on the amount of food available and the temperature. The winter increase in the death of mice was estimated by adding 0.004 to the natural rate 0.012 per day for the 90 day period of

winter. An estimate for the size of deer population per km$^2$ is taken from references on white-tailed deer (Chen et al. 2015; Hesselton and Hesselton 1982; Miller et al. 2003). In 1982, the deer density in North America was more than 3 to 4 deer per km$^2$ (Hesselton and Hesselton 1982), and the density has increased, especially in the United States. However, the deer density depends on habitat quality, and since then the densities have been regulated by harvesting management (Miller et al. 2003). The data on deer density for a given region is determined through a mandatory survey of deer hunters enforced by the Ontario Ministry of Natural Resources (Chen et al. 2015). It is assumed in our models that there are ten deer per km$^2$ because it was most often observed density based on deer hunters' responses (Chen et al. 2015). We choose a relatively high density indicative of a site where ticks and mice infection persists.

Since tick activity is regulated by temperature (Eisen et al. 2016; Ogden et al. 2004), we model the changing temperature by splitting the year into four seasons of 90 days per season. We assume spring is the first season which begins on May 1st and represents day 0 in the models (one year equals 360 days). Periodic parameters are defined to mimic the seasonality of births, feedings, and deaths (Eqs. (11)–(18)). We use trigonometric functions to generate continuous time-dependent parameters that peak in mid season, where the corresponding activity is at its highest. Equation (11) for the birth rate limits egg-laying by adults to the spring (Fig. 4a). This assumption is supported by Ogden et al. (2004) as they observed in a laboratory environment that during both hot and cold environments, females do not produce eggs or the eggs produced did not hatch. The periodic parameter for birth rate is rewritten in terms of the constant parameter $A_b$, that represents the maximum tick birth rate achieved during this 90-day period. The Eqs. (12), (14), and (16) modulate the activity levels of each stage to match their relative activity range (Fig. 1). Immature ticks of *I. scapularis* in the northeastern United States display asynchronous questing with nymphs preceding larvae (Fig. 4d) (Voordouw 2015). Adult feeding activity is limited to fall (Fig. 4c). We neglect adult feeding activity that occurs in early spring to early summer in the Northeast (Centers for Disease Control and Prevention (CDC) 2020; Eisen et al. 2016). However, the time delay with mean $\tau_A = 180$ days accounts for female adults $A_n$ that have fed, overwintered, laid eggs in the spring, and contributed to the uninfected larval stage $L_1$. Parameters $A_l$, $A_n$, and $A_a$ represent the peak feeding rates for larvae, nymphs, and adults, respectively. The death parameters for the ticks (Eqs. (13), (15), and (17)) are at their peak values $A_{l\,\max}$, $A_{n\,\max}$, and $A_{a\,\max}$, respectively, during the winter then decline during the spring. The death rate for larvae and nymphs increases again in the summer to mimic the increased death experienced by arthropods (Eisen et al. 2016). The lowest death rates are represented by $A_{l\,\min}$, $A_{n\,\min}$, and $A_{a\,\min}$. We assume that the mouse density is maintained throughout the year, with only a slight increase in the death rate over the winter by $\Delta d$. We also assume no co-feeding transmission occurs in the models (Voordouw 2015). Co-feeding transmission occurs when an infected tick co-feeds with a susceptible tick on the same host directly transmitting the infection. Co-feeding at different tick stages increases transmission and has been considered in several Lyme disease models (Nah and Wu 2021; States et al. 2017; Wu and Zhang 2020; Zhang et al. 2021).

The periodic parameters are given by the following equations:

$$b_T(t) = \max\left(A_b(2+\sqrt{2})\sin\left(\frac{\pi}{180}(t+45)\right) - A_b(\sqrt{2}+1), 0\right) \tag{11}$$

$$F_L(t) = \max\left(A_l(2+\sqrt{2})\sin\left(\frac{\pi}{180}(t-45)\right) - A_l(\sqrt{2}+1), 0\right) \tag{12}$$

$$\mu_L(t) = -\frac{A_{l\max} - A_{l\min}}{2}\sin\left(\frac{\pi}{90}t\right) + \frac{A_{l\max} + A_{l\min}}{2} \tag{13}$$

$$F_N(t) = \max\left(A_n(2+\sqrt{2})\sin\left(\frac{\pi}{180}(t+45)\right) - A_n(\sqrt{2}+1), 0\right) \tag{14}$$

$$\mu_N(t) = -\frac{A_{n\max} - A_{n\min}}{2}\sin\left(\frac{\pi}{90}t\right) + \frac{A_{n\max} + A_{n\min}}{2} \tag{15}$$

$$F_A(t) = \max\left(A_a(2+\sqrt{2})\sin\left(\frac{\pi}{180}(t-135)\right) - A_a(\sqrt{2}+1), 0\right) \tag{16}$$

$$\mu_A(t) = \frac{A_{a\max} - A_{a\min}}{2}\sin\left(\frac{\pi}{180}(t+135)\right) + \frac{A_{a\max} + A_{a\min}}{2} \tag{17}$$

$$d(t) = d_{\min} + \max\left(\Delta d(2+\sqrt{2})\sin\left(\frac{\pi}{180}(t+135)\right) - \Delta d(\sqrt{2}+1), 0\right). \tag{18}$$

The periodic parameters in Eqs. (11)–(18) are graphed over a period of two years in Fig. 4 with parameter values from Table 1. Additional details on parameter calculations can be found in Appendix B.

## 4 Mathematical Analysis

One of the fundamental ideas of disease transmission is the basic reproduction number. We apply the next generation matrix and its spectral radius from the system of differential equations (van den Driessche 2017; van den Driessche and Watmough 2002; Wang and Zhao 2008). In the next subsections, we discuss the basic reproduction number for the autonomous ODE and how to derive it in the case of the nonautonomous ODE. Also, we discuss a parameter sensitivity analysis with respect to various outcome measures.

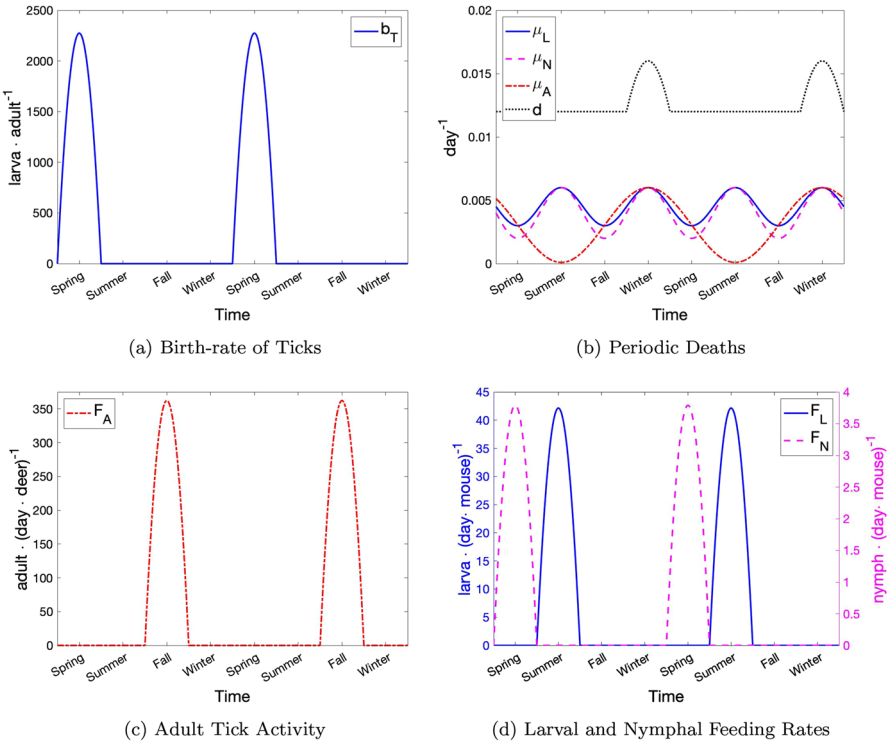


(a) Birth-rate of Ticks

(b) Periodic Deaths

(c) Adult Tick Activity

(d) Larval and Nymphal Feeding Rates

**Fig. 4** Periodic parameters graphed over two years (Color figure online)

### 4.1 Basic Reproduction Number

The basic reproduction number is a well-known threshold in epidemic models, denoted as $\mathcal{R}_0$. Biologically, this threshold is defined as the number of secondary infections caused by one infectious individual in an entirely susceptible population (Diekmann et al. 1990). If $\mathcal{R}_0$ exceeds unity, then the number of infections will grow over time, but if it is less than unity, the number will decline. Hence, the magnitude of $\mathcal{R}_0$ provides knowledge about the growth of infectious individuals at the start of an epidemic.

For the autonomous ODE with $n$ latent stages, the basic reproduction number, $\mathcal{R}_0$, can be directly calculated via the next generation matrix approach (van den Driessche and Watmough 2002). For the mouse model (2) and the tick model with latent stages (5)-(10), the infected stages are $L_1^I, \ldots, L_n^I$, $N^I$, and $M^I$. The infected stages $N_j^I$, $j = 1, \ldots, n$ do not lead to any new infections as ticks in these stages do not feed on the mouse and eventually either die or transition to adult stages. Linearization of the system of infected stages about the disease-free equilibrium (DFE) results in two matrices, $F$ and $V$. Matrix $F$ represents new infections and matrix $V$ all other transitions. The value of $\mathcal{R}_0$ is the spectral radius of the next generation matrix $FV^{-1}$:

$$\mathcal{R}_0 = \rho(FV^{-1}). \tag{19}$$

Applying the next generation matrix approach, assuming all parameters are constant, the value of $\mathcal{R}_0$ for the autonomous ODE tick-mouse model (2), (5)–(10) with $n$ latent stages results in the square root of the product of three terms, $\mathcal{R}_0 = \sqrt{(i)(ii)(iii)} = \sqrt{\mathcal{R}_0^{(n)}}$, where

$$\mathcal{R}_0^{(n)} = \underbrace{\left(\frac{\beta_L F_L L^*}{(m_L M^* + L^*)\left(d + \frac{d_D M^*}{K}\right)}\right)}_{(i)} \underbrace{\left(\frac{r_n}{r_n + \mu_L}\right)^n}_{(ii)} \underbrace{\left(\frac{\beta_M F_N M^*}{F_N M^* + \mu_N (m_N M^* + N^*)}\right)}_{(iii)}, \tag{20}$$

for $n = 1, 2, \ldots$. The mouse equilibrium value is $M^* = \frac{(b_M - d)K}{d_D}$ and the tick equilibrium values $L^*$ and $N^*$ are computed from the ODE tick model (5)–(10) when all infected states are set to zero. The parameter $r_n = n/\tau_L$, $n = 1, 2, \ldots$ is the rate of transfer between the larvae latent stages, i.e., $1/r_n = \tau_L/n$ is the average duration between the latent stages. For the special case of no delay, $n = 0$, in model (1), (2), the value of $\mathcal{R}_0^{(0)}$ is simply the product of the two terms $(i)$ and $(iii)$ in Eq. (20).

The three terms, $(i)$, $(ii)$, and $(iii)$, in $\mathcal{R}_0^{(n)}$ can be interpreted in terms of the cycle of infection from mouse to larva, larva to nymph, and nymph to mouse, respectively. Beginning from one infected mouse, the term $(i)$ is the number of larval ticks that are infected during the life of the mouse. The second term $(ii)$ is the survival of an infected larva to an infected nymph, and the third term $(iii)$ is the transmission of the infection to a susceptible mouse during infected nymph feeding. The three terms can also be interpreted beginning from an infected larva, $(ii) \to (iii) \to (i)$, or an infected nymph, $(iii) \to (i) \to (ii)$. The square root comes from the next generation matrix approach and represents the average number of secondary infections generated either from an infected mouse, an infected larva, or an infected nymph. The next generation matrix for the special case of $n = 2$ latent stages can be found in Appendix C.

For the system of DDEs (2)–(4) with constant parameters, a similar method of linearization can be used to derive the basic reproduction number provided the DFE is the same as in the ODE model, e.g., (Bai et al. 2019; Martcheva 2015). The value of $\mathcal{R}_0$ for the DDE can be directly related to that of the ODE model with $n$ latent stages. In particular, as the number of latent stages $n \to \infty$, the Erlang distribution for the delay with $n$ latent stages approaches that of a fixed delay with a Dirac delta distribution centered at the fixed delay (Bai et al. 2019; Lloyd 2001). Taking the limit as $n \to \infty$ yields

$$\mathcal{R}_0^{(n)} = \mathcal{R}_0^{(0)} \left(\frac{n/\tau_L}{n/\tau_L + \mu_L}\right)^n \to \mathcal{R}_0^{(0)} e^{-\mu_L \tau_L},$$

where $\mathcal{R}_0^{(0)} = (i)(iii)$. For a constant death rate, the survival of larvae during the delay $\tau_L$ equals $e^{-\mu_L \tau_L}$ which follows from Eq. (3). To compare the value of $\mathcal{R}_0^{(n)}$ from the ODE model to that of the DDE model, we define

$$\mathcal{R}_0^{(d)} = \left( \frac{\beta_L F_L L^*}{(m_L M^* + L^*)\left(d + \frac{d_D M^*}{K}\right)} \right) e^{-\mu_L \tau_L} \left( \frac{\beta_M F_N M^*}{F_N M^* + \mu_N (m_N M^* + N^*)} \right). \tag{21}$$

From the next generation approach, the value of $\mathcal{R}_0$ for the DDE model can be defined as $\mathcal{R}_0 = \sqrt{\mathcal{R}_0^{(d)}}$. The value of $\mathcal{R}_0^{(d)}$ is less than the value of $\mathcal{R}_0^{(n)}$. Regardless of whether the basic reproduction number is defined with or without the square root, both definitions give the same value when at the threshold value of one, i.e., $\mathcal{R}_0^{(n)} = 1 = \sqrt{\mathcal{R}_0^{(n)}}$ and $\mathcal{R}_0^{(d)} = 1 = \sqrt{\mathcal{R}_0^{(d)}}$ (Heffernan et al. 2005; van den Driessche 2017).

For the nonautonomous ODE system with periodic coefficients, similar methods and assumptions as in the autonomous case yield matrices $F(t)$ and $V(t)$ after linearization about the disease-free state (DFS) (Wang and Zhao 2008). The time variable $t$ in $F(t)$ and $V(t)$ emphasizes the time-periodic coefficients:

$$\dot{X} = (F(t) - V(t))X. \tag{22}$$

The period of the parameters is one year, simplified to $\omega = 360$ days. It is further divided into four seasons, each of length 90 days. The spectral radius cannot be directly calculated from matrices $F(t)$ and $V(t)$, as in Eq. (19). Generally, numerical methods must be applied to compute the DFS and the basic reproduction number. We describe the theoretical method from Wang and Zhao (2008) and our numerical implementation of this method. Calculation of the basic reproduction number requires the fundamental matrix solution (also called monodromy matrix) of the linear matrix system:

$$\dot{Y} = (F(t)/\lambda - V(t))Y, \qquad Y(0) = I_d, \tag{23}$$

where $I_d$ is the identity matrix and the other matrices, $Y$, $F$, and $V$, are square matrices with dimensions dependent on the number of infected states. The fundamental solution, $Y(t) = \Phi(t, \lambda)$, of Eq. (23) depends on $\lambda$ and the period $\omega$ and, therefore, so does the basic reproduction number. The value of $\lambda$ equals the basic reproduction number when the spectral radius of $\Phi(t, \lambda)$ evaluated at the period $t = \omega$ equals one. More specifically, $\lambda = \mathcal{R}_0$ if

$$\rho(\Phi(\omega, \lambda)) = 1. \tag{24}$$

The monodromy matrix is numerically solved by choosing a sequence of values $\{\lambda_i\}_{i=1}^m$ and applying a bisection algorithm until the following condition is met: $|\rho(\Phi(\omega, \lambda_i)) - 1| < 10^{-6}$. The last value $\lambda_m$ satisfying the inequality is used as the numerical approximation of the basic reproduction number, $\lambda_m \approx \mathcal{R}_0$. Additional assumptions to ensure existence and uniqueness of $\mathcal{R}_0$ as a threshold for disease outbreaks are discussed in Appendix C.

Surprisingly, the basic reproduction number as a threshold for the $n$-stage ODE model is also a threshold for the $n$-stage CTMC model with constant or periodic

coefficients (Allen and Lahodny Jr 2012; Allen and van den Driessche 2013; Bacaër and Ait Dads 2014). The basic reproduction number for the CTMC comes from a linear branching process approximation near the DFE or DFS (Allen and Lahodny Jr 2012; Allen and van den Driessche 2013; Bacaër and Ait Dads 2014; Nipa et al. 2021). Therefore, if the basic reproduction number $\mathcal{R}_0 < 1$ and the system is near the DFE or DFS, the ODE model predicts that the disease dies out and the CTMC predicts that the disease dies out with probability one. However, if $\mathcal{R}_0 > 1$, the ODE always predicts a disease outbreak, a rise in number of cases, but in the CTMC model this is not the case. In the CTMC model, there is a positive probability $p$ of no disease outbreak and a positive probability of $1 - p$ of a disease outbreak. In the case of periodic parameters, the probability $p$ depends on the time infection is introduced and the number of infected mice and ticks, e.g., (Bacaër and Ait Dads 2014; Nipa et al. 2021).

### 4.2 Parameter Sensitivity

To determine the relative importance of each parameter, we conduct a sensitivity analysis. We discuss the method here and apply this method in Sect. 5.3 to determine the parameters with the largest effect on $\mathcal{R}_0$ at the DFS and on nymph infection prevalence (NIP), mouse infection prevalence (MIP), and density of infected nymphs per km$^2$ (DIN) at the endemic state of the ODE model:

$$\text{NIP} = \frac{N^I}{N^I + N^S}, \qquad \text{MIP} = \frac{M^I}{M^I + M^S}, \qquad \text{DIN} = N^I.$$

As these expressions vary with time, we compute their maximum and minimum values.

In particular, we estimate what is sometimes referred to as an *elasticity index* of specific quantities of interest, $Q$ ($\mathcal{R}_0$, NIP, MIP, DIN), with respect to a parameter $p$, as described in references (Chitnis et al. 2008; Sauvage et al. 2003; van den Driessche 2017) The elasticity index of $Q$ with respect to parameter $p$ is defined as

$$\frac{\partial Q}{\partial p}\frac{p}{Q}.$$

The nonautonomous ODE has no explicit expression for $\mathcal{R}_0$ or infection prevalences. These expressions are calculated numerically for a given set of parameter values. Therefore, we follow the analysis from Sauvage et al. (2003) to approximate the elasticity index or sensitivity of a parameter with respect to a proportional change in the parameter $p$, i.e., $\partial Q/\partial p \approx \Delta Q/\Delta p$, where $\Delta Q = Q(p + \Delta p) - Q(p)$. For example, if there is an increase of $p$ by 10%, $\Delta p = 0.1p$, the elasticity index simplifies to

$$\frac{\partial Q}{\partial p}\frac{p}{Q} \approx \frac{\Delta Q}{\Delta p}\frac{p}{Q} = \frac{Q(1.1p) - Q(p)}{0.1Q(p)}.$$

In Sect. 5.3, we focus on the nonautonomous ODE model with 100 latent stages.

## 5 Numerical Results for ODE and DDE

In this section, we present numerical results based on the parameter values given in Table 1 and in Fig. 4. First, values for the basic reproduction number for the various models are computed. Second, the solution of the ODE model is compared to the DDE model. As the number of latent stages increases, there is closer agreement between the two models. Lastly, for the nonautonomous ODE model, we compute the sensitivity of model parameters to $\mathcal{R}_0$, to the maximum and minimum of NIP and DIN, and the maximum of MIP.

### 5.1 $\mathcal{R}_0$ Calculations

For the autonomous ODE and DDE with constant coefficients, the explicit values for the DFE and the reproduction numbers can be calculated from the parameter values defined in Table 1 and the formulas in Sect. 4.1. In particular, for $\beta_M = 0.75$ and $\beta_L = 1$, the basic reproduction numbers for the autonomous DDE and ODE models with $n = 2$, 10 or 100 latent stages are in close agreement, that is,

$$\sqrt{\mathcal{R}_0^{(d)}} \approx 4.996 \approx \sqrt{\mathcal{R}_0^{(n)}}, \quad n = 2, 10, 100.$$

The preceding expression for $\mathcal{R}_0^{(n)}$ from Eq. (20) does not give the correct value for the nonautonomous ODE model with periodic coefficients. The basic reproduction numbers are computed numerically using the method described in Sect. 4.1 (Wang and Zhao 2008). Before conducting this calculation we must ensure that seven assumptions (A1)–(A7) are satisfied. The first five assumptions are straightforward. Assumptions (A6) and (A7) require stability of the DFS and an assumption regarding matrix $-V(t)$ (Wang and Zhao 2008). These assumptions are discussed in Appendix C.

Applying the methods from Sect. 4.1 and matrix Eq. (23) for the nonautonomous ODE model with $n$ latent stages, the basic reproduction numbers are

$$\sqrt{\mathcal{R}_0^{(2)}} \approx 5.056, \ \sqrt{\mathcal{R}_0^{(10)}} = 5.201, \ \sqrt{\mathcal{R}_0^{(100)}} = 5.213.$$

### 5.2 DDE and ODE Simulations

The DDE model is solved with dde23 in MATLAB and the ODE model is solved with ode45 in MATLAB using parameter values defined in Table 1 and periodic functions described in Fig. 4. The larva, nymph, and adult tick stages ($L$, $N$ and $A$) and mice ($M$) are plotted over 14 years in Fig. 5. Graphs of the ODE for $n = 2$ or 10 latent stages are in Appendix D. The ODE solution approaches that of DDE as $n$ approaches infinity. After 12 years the population densities for both the DDE and the ODE ($n = 100$ latent stages) models have reached an endemic periodic solution. The minimum and maximum densities of infected nymphs (DIN) at the ODE endemic solution are approximately 2.5 and 8.4 nymphs per square meter, respectively (converted from densities per km$^2$). The NIP values range between 0.40 and 0.51 while the MIP values fluctuate between

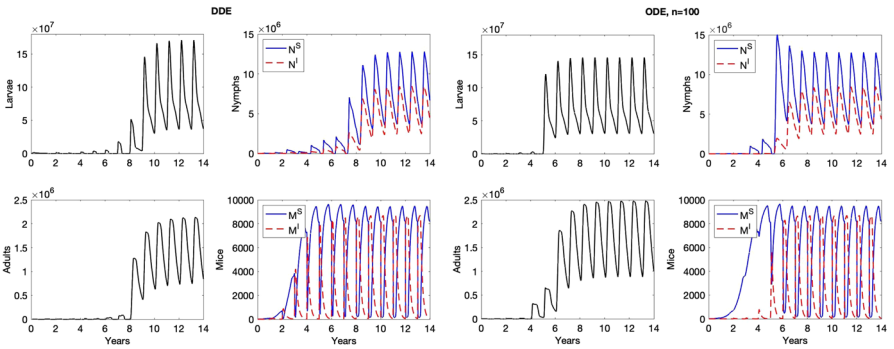


**Fig. 5** DDE solution is compared with the ODE solution with $n = 100$ latent stages. Baseline parameters are given in Table 1 and initial conditions are $L(0) = 1000$, $N(0) = 100$, $A(0) = 20$, $M(0) = 10$, $M^I(0) = 2$, with all other initial conditions set to zero. Plots of larvae and adults over time are the stages $L$ and $A$ (Color figure online)

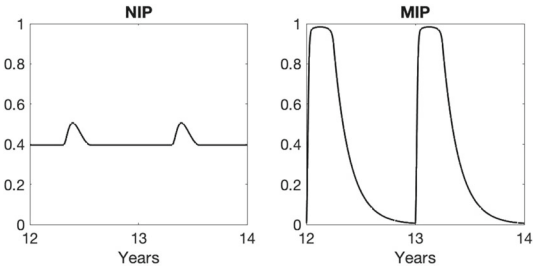


**Fig. 6** NIP and MIP at the endemic periodic solution of the ODE in Fig. 5 with $n = 100$ latent stages

0.005 and 0.98 (Fig. 6). These values for NIP are biologically reasonable, but DIN values are relatively high (Keesing et al. 2009; LoGiudice et al. 2003; Ogden et al. 2007). Estimates of NIP from various field studies range from 0.186 to about 0.90 (LoGiudice et al. 2003; Ogden et al. 2007). Keesing et al. (2009) give estimates of DIN based on the number of questing nymphs and available hosts that range from 2000 to 8000 per hectare (0.2–0.8 per square meter). If our population densities are measured in 10 $km^2$ instead of 1 $km^2$ or if the mouse carrying capacity is reduced by a factor of 0.1 (parameter $K$ multiplied by 0.1), then there is no change in NIP, MIP or $\mathcal{R}_0$, but our DIN values decrease by a factor of 0.1 and agree with those in Keesing et al. (2009).

The assumptions on seasonal variations and diapause delays between tick stages in the two-year tick cycle drive the seasonal infection pattern seen in the ODE model in Fig. 7. In the spring, infection is spread from infected nymphs to mice and in the summer, infection is spread from infected mice to larvae (feeding activity in Fig. 4d). Then nymph infection peaks at the end of the summer. Reasons for the high DIN estimates from our ODE model may be that the model accounts for all infected nymphs which would likely be larger than the number based on field estimates and also infected nymphs peak in late summer in our model, after questing and feeding activity in the spring (Fig. 7).

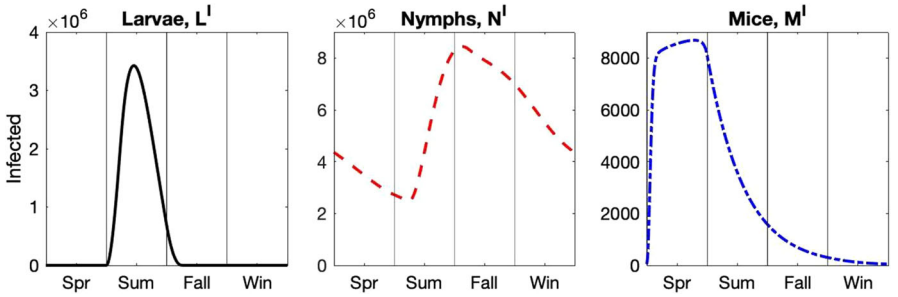


**Fig. 7** Dynamics of the periodic densities of infected larvae, nymphs, and mice ($L^I = \sum_{j=1}^{100} L_j^I$, $N^I$, and $M^I$) at the endemic ODE solution during spring, summer, fall and winter, as shown in Fig. 5. Stage $L^I$ is the sum of all infected larval stages after feeding on mice. That is, $L_1^I$ is the newly infected stage and stages $L_j^I$, $j = 2, \ldots, n$ are the latent stages until transition to nymph (Color figure online)

### 5.3 Parameter Sensitivity

A parameter sensitivity analysis is performed on the nonautonomous ODE model to assess the effect of a change in parameters on the following outcome measures: $\mathcal{R}_0$, NIP, MIP, and DIN. Parameter values are increased by 10% from their baseline values in Table 1 (except $\beta_L$ is decreased by 10%), and the relative change in the outcomes recorded in Fig. 8. Maximum and minimum values are recorded for NIP and DIN, but only the maximum values for MIP as the minimum values are very close to zero. The sensitivity of the maximum values of MIP are relatively small and not as sensitive when compared to the other outcomes (Fig. 8). Therefore, we discuss the parameter sensitivity with respect to the three outcome measures, $\mathcal{R}_0$, NIP, and DIN.

Based on the sensitivity analysis, parameters related to birth, death, feeding and transmission have the greatest impact on the three outcome measures. Outcomes NIP and $\mathcal{R}_0$ are highly sensitive to the parameter for the probability of transmission from infected mice to larvae, $\beta_L$. The outcome NIP is not as sensitive to other parameters. However, surprisingly, an increase in nymphal death rates, $A_{n\max}$ and $A_{n\min}$, increases the maximum value of NIP but has the opposite effect on the minimum value of NIP. A potential explanation for this behavior is that the nymphal death rate allows more turnover in the population. What we observe may be explained by the bottleneck effect (Novella et al. 1999). The infection is not detrimental to the nymph. When there is more turnover in the population, there is a chance that the infection dies out, or that the decrease in population causes a bottleneck and increases the infection. The basic reproduction number $\mathcal{R}_0$ is also highly sensitive to parameters for the competency of transmission from infected nymphs to mice, $\beta_M$, the maximum nymphal feeding rate, $A_n$, and the mouse birth rate, $b_M$. The impact of some of these parameters can be seen in the constant parameter case in the definition of $\mathcal{R}_0^{(n)}$ in Eq. 20. The outcome measure DIN is highly sensitive to $\beta_L$ but not to $\beta_M$ and sensitive to the mouse parameters for carrying capacity, birth and death rates, $K$, $b_M$, $d_M$, and $d_{\min}$, as well as the maximum values for larval feeding rate, $A_l$, and maximum nymphal death rate, $A_{n\max}$. The

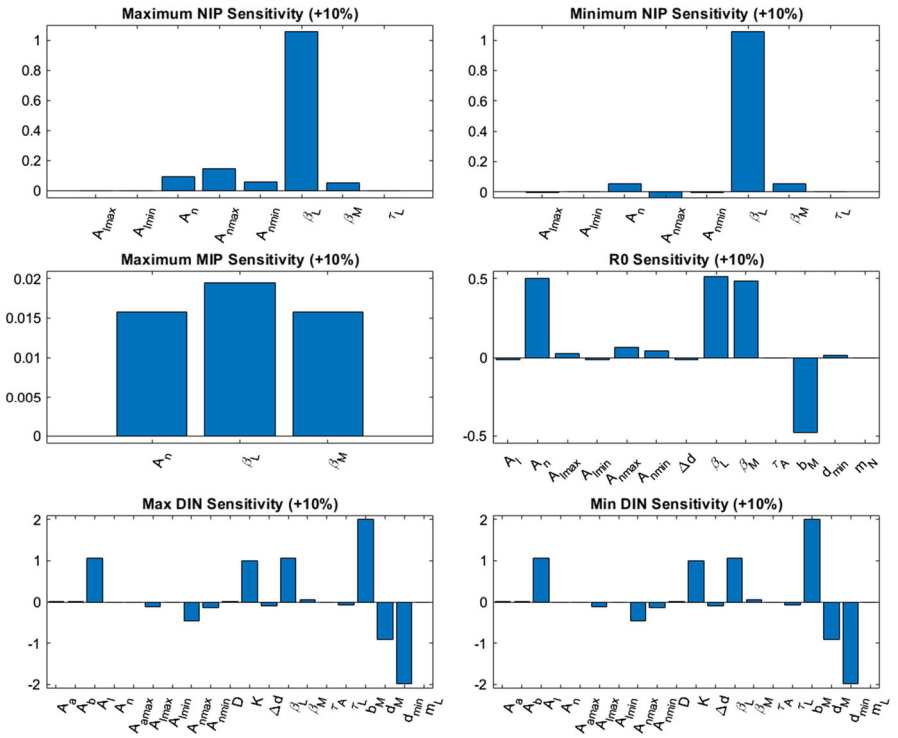


**Fig. 8** Sensitivity analysis of maximum and minimum of NIP, maximum and minimum of DIN, and maximum of MIP at the endemic state and of $\mathcal{R}_0$ at the disease-free state for various parameter values of the nonautonomous ODE model with 100 latent stages. Parameter values are increased by 10% of their baseline values in Table 1 with the exception of $\beta_L$ which is decreased by 10%. Sensitivity greater than $10^{-3}$ is shown (Color figure online)

significant role played by the mouse parameters is reasonable as nymph and larva are dependent on the mouse for survival and for infection.

## 6 Numerical Results for CTMC

One of the advantages of the CTMC model is its ability to account for seasonal and demographic variability in the real world. Harsh winters, food distribution, and death of infected individuals before they pass on the infection can result in the infection dying out in the tick and mouse populations. We apply the CTMC model to investigate the effects of seasonal and demographic variability on the establishment of *B. burgdorferi* infection in tick and mice populations. The basic reproduction number for the CTMC model is the same as the ODE model when tick and mice populations are at the DFS (Bacaër and Ait Dads 2014). When $\mathcal{R}_0 > 1$, in the ODE model, the system reaches an endemic state, but in the CTMC model, there is a positive probability that the infection will die out and not spread. We introduce a small number of ticks and mice (not at the DFS) into a new site that has the potential to support both ticks and mice

at an endemic state ($\mathcal{R}_0 = 5.213 > 1$). One or two infected mice or nymphs are also introduced to the site. In a seasonally varying CTMC model, whether the infection dies out depends on the time of year and the number of infected ticks and mice that are introduced. As the tick and mice populations are not at the DFS, the two populations are growing. The question we address is: Do these growing tick and mice populations support populations of infected ticks and mice up to one year after introduction?

First, we illustrate the dynamics of the ODE solution and several CTMC sample paths when ticks and mice are introduced into a site that does not contain ticks or mice. Second, we perform numerical simulations of the CTMC model to investigate whether *B. burgdorferi* infection will persist in the population for up to one year when a few infected ticks or mice are also introduced at the same time. To investigate seasonal effects, infected ticks and mice are introduced at the beginning of one of the four different seasons.

### 6.1 ODE and CTMC Simulations

In this section we observe how low infection in the initial conditions can either result in the infection in the CTMC model persisting or dying out, even when the ODE model shows an infection outbreak (Fig. 9). The initial conditions for the ODE and CTMC models are 1000 larvae, 100 nymphs, 20 adults, and 10 mice with 2 infected mice introduced at $t = 90$ days (beginning of summer). The initial tick and mice populations are sufficiently large such that the populations continue to grow in both the ODE and CTMC models (although the infection may die out in the CTMC model). The ODE solution converges to an annual cyclical pattern as shown in Fig. 5. The three sample paths of the CTMC illustrate the variability inherent in the stochastic process. A close-up view of the infected ticks and mice in the ODE and CTMC models from Fig. 9 are shown in Fig. 10. Larvae feed on available mice and if the mice are infected, larvae become infected (Fig. 10). The larvae that have fed molt to susceptible or infected nymphs. Nymphs only take blood meals in spring. Thus, nymphs that survive through winter to the beginning of spring in the next year (day 360) feed on mice and molt to adults. The few adults at the beginning of the summer, day 90, die by the end of the summer, day 180. Unlike ticks which reproduce in spring, mice reproduce all year round. Therefore, in Fig. 9 (CTMC, lower right) with a small and growing mouse population, the variability in births and deaths is more visible in the mouse population than in the tick populations. For this particular example, the three sample paths follow similar patterns to that of the ODE dynamics as there is a low probability of the infection dying out in this case. When the ODE infection dynamics are close to zero, the CTMC model may result in disease extinction. Figure 11 illustrates eight cases of the ODE infection dynamics, when either infected nymphs or infected mice are introduced at $t_0 = 0, 90, 180, 270$ days (beginning of spring, summer, fall, or winter, respectively). It can be seen that the season of introduction has an impact on the number of infections and that it differs depending on which species carries the infection. This will be helpful in interpreting the results on the probability of disease extinction in the next section.

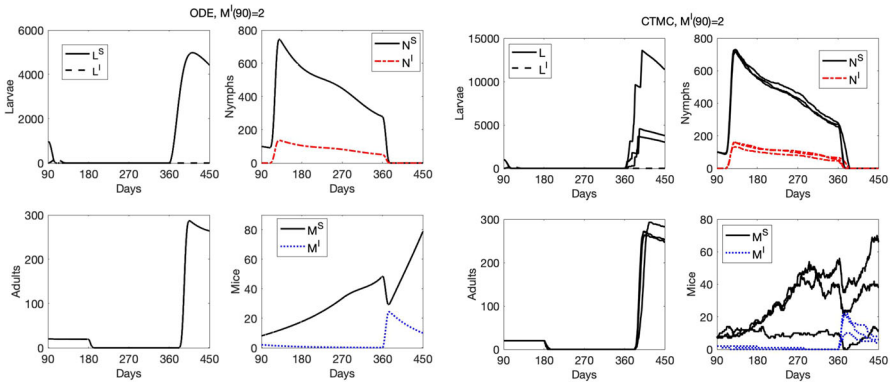


**Fig. 9** The ODE solution and three sample paths of the CTMC model with $n = 100$ latent stages are graphed over one year, $t \in [90, 450]$ days. Initial conditions at $t = 90$ days are $L(90) = 1000$, $N(90) = 100$, $A(90) = 20$, $M(90) = 10$, and $M^I(90) = 2$. All other initial conditions for the tick stages at $t = 90$ are set to zero (Color figure online)

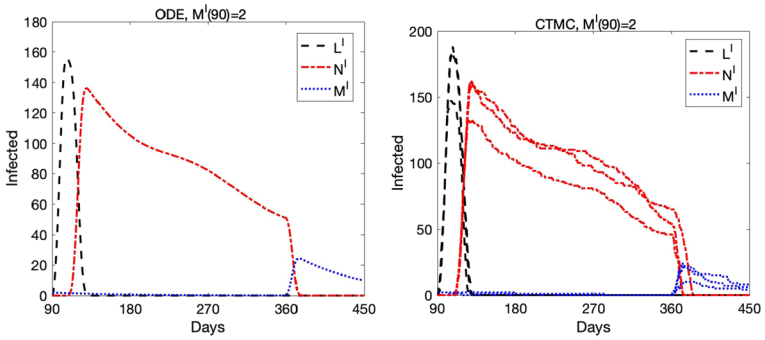


**Fig. 10** Close-up view from Fig. 9 of the infected tick and mouse stages of the ODE solution and the three sample paths of the CTMC model over the time interval [90, 450] days (Color figure online)

## 6.2 Probability of Extinction

A key assumption is that the environment is clear of mice and ticks. However, the environment is capable of supporting both infected ticks and infected mice as demonstrated in the solutions graphed in Fig. 5. The question we address is the following: Does introduction of mice and ticks, a few of which are infected, result in persistence of the infection into the next year? As can be seen in Fig. 11 as well as Tables 3 and 4, the timing of introduction and the species carrying the infection affect the infection dynamics. If the infection persists through the first year, it is more likely to continue through the following year, thus increasing the chance of becoming endemic in the population. The probabilities of disease extinction in the Tables 3 and 4 are estimated from running 500 sample paths of the CTMC and computing the proportion of those paths when the infection in both ticks and mice has reached zero before the end of one year (no infected ticks or mice remain in the populations).

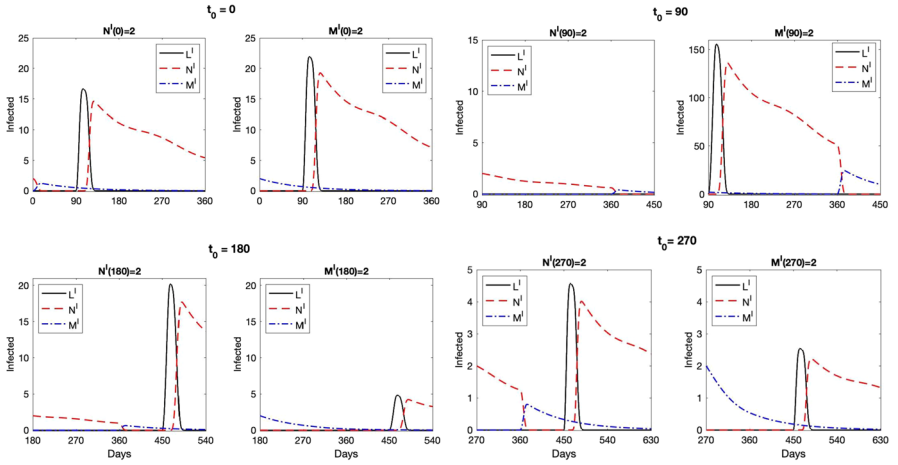


**Fig. 11** ODE solutions of the infected larvae $L^I$, nymph $N^I$, and mice $M^I$ with initial conditions dependent on the season: $L(t_0) = 1000$, $N(t_0) = 100$, $A(t_0) = 20$, $M(t_0) = 10$ for $t_0 = 0, 90, 180, 270$ and with either two infected nymphs or two infected mice, $N^I(t_0) = 2$ or $M^I(t_0) = 2$ ($L^I = \sum_{j=1}^{100} L_j^I$). Vertical scales for $t_0 = 90$ differ (Color figure online)

**Table 3** Summary of probability of disease extinction with the mean and the standard deviation (SD) of the time until extinction (in days) when one or two infected nymphs are introduced at the start of each season, spring ($t_0 = 0$), summer ($t_0 = 90$), fall ($t_0 = 180$) and winter ($t_0 = 270$). Initial conditions are $L(t_0) = 1000$, $N(t_0) = 100$, $A(t_0) = 20$, and $M(t_0) = 10$ with either $N^I(t_0) = 1$ or 2

| Infection introduced | Time of introduction | Season of extinction | Prob. of extinction | Mean time (SD) until extinction |
|---|---|---|---|---|
| $N^I = 1$ | Spring | Spring | 0.776 | 29.15 (20.20) |
| | Summer | Fall | 0.924 | 150.61 (106.38) |
| | Fall | Winter | 0.866 | 136.43 (67.03) |
| | Winter | Winter | 0.830 | 80.26 (41.90) |
| $N^I = 2$ | Spring | Spring | 0.632 | 29.95 (26.11) |
| | Summer | Winter | 0.826 | 208.39 (92.65) |
| | Fall | Winter | 0.798 | 176.51 (45.59) |
| | Winter | Spring | 0.726 | 103.36 (33.36) |

When infected nymphs are introduced at $t_0 = 90$ the ODE solution in Fig. 11 illustrates the number of infected nymphs reach values less than one. A high probability of disease extinction can be observed in the CTMC simulations as shown in Table 3. The probabilities of extinction, 0.9240 with one infected nymph or 0.826 with two infected nymphs, are the highest probabilities of extinction when infected nymphs are the mode of infection. Alternatively, when infected mice are introduced at $t_0 = 90$ (summer), infected nymphs are produced after the infected larvae peak, as shown in Figs. 10 or 11. Disease extinction within that first year is very low, probability 0.056 with one infected mouse or 0.004 with two infected mice. Also, notable is that introduction of infected nymphs or infected mice at the beginning of summer, $t_0 = 90$,

**Table 4** Summary of probability of extinction and mean time and standard deviation (in days) until extinction when one or two infected mice are introduced at the start of each season. Initial conditions are $L(t_0) = 1000$, $N(t_0) = 100$, $A(t_0) = 20$, and $M(t_0) = 10$ with $M^I(t_0) = 1$ or 2 for $t_0 = 0 =$ spring, 90 = summer, 180 = fall, 270 = winter

| Infection introduced | Time of introduction | Season of extinction | Prob. of extinction | Mean time (SD) until extinction |
|---|---|---|---|---|
| $M^I = 1$ | Spring | Spring | 0.690 | 37.39 (29.95) |
| | Summer | Fall | 0.056 | 173.03 (159.43) |
| | Fall | Winter | 0.964 | 72.10 (59.85) |
| | Winter | Spring | 0.902 | 51.18 (42.39) |
| $M^I = 2$ | Spring | Spring | 0.414 | 52.97 (23.51) |
| | Summer | Winter | 0.004 | 296.35 (47.17) |
| | Fall | Spring | 0.964 | 100.84 (57.60) |
| | Winter | Winter | 0.856 | 80.81 (45.70) |

results in the longest duration of persistent infection before disease extinction (mean time to extinction).

Biologically this result makes sense as at $t_0 = 90$ the environment is optimal for larvae and nymphs to survive and larvae to take blood meals. Higher tick densities means more opportunities for infection. The infection takes off because a primary magnifying host is present as well as multiple larvae to feed on the infected mice that then molt into infected nymphs. The subsequent decline in the nymph population is due to their transition to the adult stage, and then the cycle begins again. The estimates for probability of extinction in Tables 3 and 4 are robust to an increase in the initial conditions for susceptible number of ticks and mice. Estimates were checked with initial conditions increased by a factor of two. The estimates are sensitive to the season of introduction and the number of infected mice and nymphs.

The most important take-away messages from Tables 3 and 4 are that it only takes a few infected nymphs to result in a positive probability of maintaining the infection for at least one year and the presence of infected mice at the beginning of spring can maintain and amplify the infection. Also, if many infected nymphs are introduced (e.g., via migrating birds) and mice are available, the probabilities of extinction can be much smaller than those in Table 3.

## 7 Discussion

The major goals of this investigation are to formulate a realistic model for the two-year tick-mouse cycle for Lyme disease and to demonstrate the impact of seasonality on the occurrence and prevalence patterns of Lyme disease. It has been observed in field experiments that all aspects of tick-borne diseases are influenced by seasons (Apanaskevich and Oliver 2013; Eisen et al. 2016; Lou et al. 2014). Lyme disease poses unique public health problems as the symptoms of Lyme disease if not caught early can lead to chronic illness and death (Centers for Disease Control and Prevention (CDC)

2021; Schwartz et al. 2017). In the United States, Lyme disease is the most common vector-borne disease (Centers for Disease Control and Prevention (CDC) 2020). One of the goals of the Centers for Disease Control and Prevention's TickNET program is to improve surveillance in areas with endemic Lyme disease as well as investigating the spread of Lyme disease into land that borders endemic regions (Centers for Disease Control and Prevention (CDC) 2021; Schwartz et al. 2017).

In our models, seasonal variation is included through births, deaths, and tick feeding as well as three diapause delays between tick stages: larva, nymph, and adult. A DDE with fixed delays is extended to a more realistic Erlang distribution which is incorporated in the ODE and CTMC models. These latter two models are used to investigate the seasonal effects on the dynamics of the tick-mouse cycle (Figs. 9, 10 and 11). As the CTMC model includes both demographic and seasonal variability, it is also used to estimate the seasonal probability that *B. burgdorferi* infection can be established in the tick-mouse cycle one year after its introduction (Tables 3 and 4). Importantly, for infected tick and mice populations to become established, a suitable habitat must be available for the two host reservoirs, mice and deer. We assumed this was the case where the basic reproduction number for the ODE model is greater than 5. In this environment, our numerical results indicate that the introduction of a few infected mice or infected ticks has the potential to result in a sustained infection. Introduction of infected mice during summer when larvae numbers are at their peak results in the lowest probability of disease extinction (highest probability of a sustained infection in mice and ticks).

The chance of infection becoming endemic in an area is dependent on the season. For example, if infected ticks are brought into a disease-free area during spring bird migration there is a chance the infection becomes endemic in the population (Becker and Han 2021; Heffernan et al. 2014; Ogden et al. 2008; Wu et al. 2016). Other seasonal influences that impact Lyme disease include mast cycles that serve as important food resources for both mice and deer (Jones et al. 1998; Ostfeld et al. 2006, 1996). Masting is the production of acorns over a multi-year period with the amount being produced fluctuating each year. Fluctuations in mice populations driven by masting cycles add another layer of seasonality to the tick-mouse cycle. This has been shown in other zoonotic diseases where the mouse serves as a reservoir (Abramson and Kenkre 2002; Pittman 2022; Sauvage et al. 2003). Habitat differences and the additional fluctuation of mice and deer populations change food availability and create an environmental pressure that impacts reproduction, death, and population densities (Allan et al. 2003). The feeding activities of the three tick stages (Fig. 4c, d) and the delays ensure a two-year tick life cycle in our model. However, our model restricts adult feeding activity to the fall and does not account for adult feeding in early spring to early summer in the Northeast (Centers for Disease Control and Prevention (CDC) 2020; Eisen et al. 2016). Infected adults do not pass the infection to eggs. Therefore, whether this restriction has an impact on the tick-mouse disease dynamics needs further investigation. These seasonal environmental factors and other features unique to the spread of Lyme disease in specific regions, such as co-feeding transmission and adult feeding activity, are important to include in developing more realistic stochastic tick-mouse models (Eisen et al. 2016; Wu and Zhang 2020).

In the sphere of public health, it is important for the local health departments to be aware of, and to share with the public, information concerning seasonal trends in Lyme disease. Periodic parameters model seasonality of tick birth and death rates as well as feeding rates (Fig. 4) and follow the two-year tick life cycle (Fig. 1). In areas where there are data available on weather and tick activity the periodic parameters may be tailored for further application in the field of epidemiology (Gaff et al. 2020). Based on the numerical results of the ODE and CTMC models, prevention of the spread of infected mice (or other competent reservoirs) into new regions during the summer is an important control measure for Lyme disease.

**Acknowledgements** This research was part of the 2021 Summer Research Experiences for Undergraduates (Husar et al. 2021), hosted by Texas Tech University and funded by the National Science Foundation under Grant # DMS-2050133. We thank the reviewer for many helpful suggestions.

**Author Contributions** Authors KH, DCP, and JR contributed to the formulation and analysis of the models and wrote the numerical codes; KH, DCP, JR, and LJSA did the computations and the graphics. LJSA directed the research. All authors contributed to the literature search and wrote the paper.

**Code Availability** Codes are written in MATLAB-R2021a under Texas Tech University authorized licence. To receive a copy of a MATLAB code, please contact the authors.

## Declarations

**Conflict of interest** The authors declare that they have no conflict of interest.

## Appendix A: Erlang Distribution

In the DDE model, the three delays follow a Dirac delta distribution with means equal to $\tau_L$, $\tau_N$, or $\tau_A$. We approximate the fixed delay in the DDE model with $n$ latent stages in the ODE model. This results in an Erlang distribution for each delay (Lloyd 2001). Using $n$ latent stages instead of fixed delays allows for a more realistic description of the transition of ticks between stages, as the number of days between stages is not the same for all ticks.

We demonstrate for the larval delay $\tau_L$ that the $n$ latent stage ODE model results in a delay having an Erlang distribution with mean $\tau_L$ and variance $\tau_L^2/n$. Let $r = n/\tau_L$ be the rate of transfer between the $n$ larval latent stages, $L_i, i = 1, \ldots, n$. Let $L_1(0) = L_0$ be the initial number of larvae in stage $L_1$ and zero in the remaining stages. Then the transitions are $L_1 \to L_2 \to \cdots \to L_n \to N$. The differential equations for these stages with no deaths are

$$\begin{aligned}
\frac{dL_1}{dt} &= -rL_1 \\
\frac{dL_2}{dt} &= rL_1 - rL_2 \\
&\vdots \\
\frac{dL_n}{dt} &= rL_{n-1} - rL_n
\end{aligned}$$

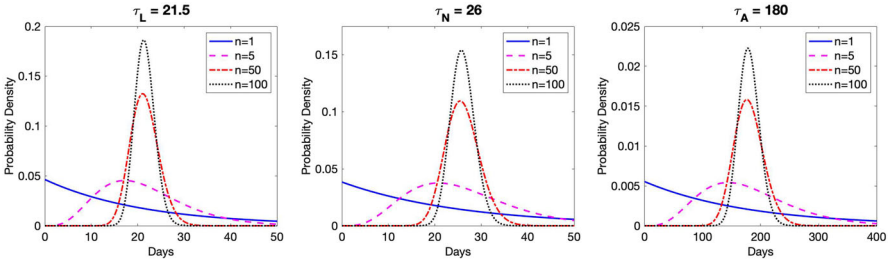


**Fig. 12** Erlang distribution for different values of $n$ and $\tau$ (Color figure online)

$$\frac{dN}{dt} = rL_n.$$

Solving the system of equations leads to $L_n(t) = L_0 r^{n-1} t^{n-1} e^{-rt}/(n-1)!$. Thus, the probability that a larva at the $n$ stage enters the nymph stage at time $t$ without dying is $rL_n(t)/L_0$, which equals

$$\frac{r^n t^{n-1} e^{-rt}}{(n-1)!}, \quad t > 0.$$

The preceding expression defines the probability density of the gamma distribution or more specifically, since the number of latent stages is a positive integer, it is an Erlang distribution with mean $n/r = \tau_L$ and variance $n/r^2 = \tau_L^2/n$. Figure 12 presents an illustration of the convergence of the Erlang distribution to the Dirac delta distribution as $n$ increases.

## Appendix B: More on Parameters

We assume the average number of eggs deposited is 3000 eggs per female tick (Lindsay et al. 1995). The experiment conducted by Lindsay et al. (1995) was a combination of field study and lab data. The average number of eggs laid per female ticks was determined by counting the eggs after being deposited. We assume that half of the population of adult ticks are females. Thus, we expect an average of 1500 eggs per adult tick. Next, we calculate the value of $A_b$ in Eq. (11) so that the average birth rate $b_T$ during the period of 90 days in the spring equals 1500. That is,

$$\frac{1}{90}\int_0^{90} A_b\left[(\sqrt{2}+2)\sin\left(\frac{\pi}{180}(t+45)\right) - (\sqrt{2}+1)\right]dt = 1500$$

$$A_b\int_0^{90}\left[(\sqrt{2}+2)\sin\left(\frac{\pi}{180}(t+45)\right) - (\sqrt{2}+1)\right]dt = 135,000$$

$$A_b\left(\frac{360(1+\sqrt{2})}{\pi} - 90(1+\sqrt{2})\right) = 135,000$$

$$A_b = \frac{135,000\pi}{(360 - 90\pi)(1+\sqrt{2})}$$
$$A_b \approx 2273.9035.$$

We assume the average feeding rate of larvae on a mouse is $27.8\frac{\text{larva}}{\text{mouse·day}}$ as in reference LoGiudice et al. (2003). To find the value of $A_l$, we set the average value of $\beta_L(t)$ during the summer (when it is non-zero) to the average feeding rate. Thus,

$$\frac{1}{90}\int_{90}^{180} A_l\left[(\sqrt{2}+2)\sin\left(\frac{\pi}{180}(t-45)\right) - (\sqrt{2}+1)\right]dt = 27.8$$
$$A_l\int_{90}^{180}\left[(\sqrt{2}+2)\sin\left(\frac{\pi}{180}(t-45)\right) - (\sqrt{2}+1)\right]dt = 27.8\cdot 90$$
$$A_l\left(\frac{360(1+\sqrt{2})}{\pi} - 90(1+\sqrt{2})\right) = 27.8\cdot 90$$
$$A_l = \frac{27.8\cdot 90\pi}{(360-90\pi)(1+\sqrt{2})}$$
$$A_l \approx 42.1430.$$

Calculation of $A_n$ and $A_a$ are similarly defined as $A_l$, except that feeding occurs in the spring and fall, respectively. The average feeding rate for nymph is $2.5\frac{\text{nymph}}{\text{mouse·day}}$ as given in reference Ogden et al. (2005) and for adults it is $239\frac{\text{adult}}{\text{deer·day}}$ as in reference LoGiudice et al. (2003). This results in the following formulas for $A_n$ and $A_a$:

$$\frac{1}{90}\int_{0}^{90} A_n\left[(\sqrt{2}+2)\sin\left(\frac{\pi}{180}(t+45)\right) - (\sqrt{2}+1)\right]dt = 2.5$$
$$A_n\int_{0}^{90}\left[(\sqrt{2}+2)\sin\left(\frac{\pi}{180}(t+45)\right) - (\sqrt{2}+1)\right]dt = 2.5\cdot 90$$
$$A_n\left(\frac{360(1+\sqrt{2})}{\pi} - 90(1+\sqrt{2})\right) = 2.5\cdot 90$$
$$A_n = \frac{2.5\cdot 90\pi}{(360-90\pi)(1+\sqrt{2})}$$
$$A_n \approx 3.7898$$

and

$$\frac{1}{90}\int_{180}^{270} A_a\left[(\sqrt{2}+2)\sin\left(\frac{\pi}{180}(t-135)\right) - (\sqrt{2}+1)\right]dt = 239$$
$$A_a\int_{180}^{270}\left[(\sqrt{2}+2)\sin\left(\frac{\pi}{180}(t-135)\right) - (\sqrt{2}+1)\right]dt = 239\cdot 90$$
$$A_a\left(\frac{360(1+\sqrt{2})}{\pi} - 90(1+\sqrt{2})\right) = 239\cdot 90$$

$$A_a = \frac{239 \cdot 90\pi}{(360 - 90\pi)(1 + \sqrt{2})}$$
$$A_a \approx 362.3086.$$

The average mouse litter size is about 4.5 mice (Centers for Disease Control and Prevention (CDC) 2023). A female mouse has an average of 3 litters per year (Centers for Disease Control and Prevention (CDC) 2023). Assuming that half of the mice population is female, the birth rate for mice is $b_M = \frac{4.5 \cdot 3}{2 \cdot 360} = 0.01875$ day$^{-1}$, where we divide by 360 to get a daily rather than a yearly rate. The mouse population density varies significantly, and reaches a maximum of approximately 12,000 mice per square kilometer (Vessey 1987). Thus, we choose $K = 150$, as this value results in an average density of about 10,000 mice at the carrying capacity (Fig. 5).

## Appendix C: Next Generation Matrix

To calculate the basic reproduction number for the ODE model with $n$ latent stages, the next generation matrix approach (van den Driessche and Watmough 2002; Wang and Zhao 2008) is applied. Two matrices, $F$ and $V$, need to be calculated from the system of the infected stages $L_1^I, \ldots, L_n^I$, $N^I$, and $M^I$ at the disease-free solution. For the autonomous ODE, the value of $\mathcal{R}_0$ is the spectral radius of the next generation matrix $FV^{-1}$, $\mathcal{R}_0 = \rho(FV^{-1})$. Matrix $F$ represents new infections and matrix $V$ all other transitions.

For the case $n = 2$, we let $r_2 = \frac{2}{\tau_L}$ with matrices $F$ and $V$ defined as follows:

$$F = \begin{pmatrix} 0 & 0 & 0 & \frac{\beta_L F_L L^*}{m_L M^* + L^*} \\ 0 & 0 & 0 & 0 \\ 0 & 0 & 0 & 0 \\ 0 & 0 & \frac{\beta_M F_N M^*}{m_N M^* + N^*} & 0 \end{pmatrix}$$

and

$$V = \begin{pmatrix} \mu_L + r_1 & 0 & 0 & 0 \\ -r_1 & \mu_L + r_2 & 0 & 0 \\ 0 & -r_2 & \frac{F_N M^*}{m_N M^* + N^*} + \mu_N & 0 \\ 0 & 0 & 0 & d + \frac{d_D M^*}{K} \end{pmatrix}.$$

Applying these two matrices, the next generation matrix $FV^{-1}$ for the autonomous ODE equals

**Table 5** Autonomous ODE and DDE disease-free equilibria based on the average parameter values in Table 1

| ODE $n$ stages | $L$ | $N^S$ | $A$ | $M$ |
|---|---|---|---|---|
| 2 | $1.665888479 \times 10^7$ | $1.279694563 \times 10^7$ | $1.488740226 \times 10^6$ | 9135.795 |
| 10 | $1.520073663 \times 10^7$ | $1.275092712 \times 10^7$ | $1.485237124 \times 10^6$ | 9135.795 |
| 100 | $1.482789479 \times 10^7$ | $1.273914913 \times 10^7$ | $1.484423091 \times 10^6$ | 9135.795 |
| DDE | $1.478528600 \times 10^7$ | $1.273779958 \times 10^7$ | $1.484332029 \times 10^6$ | 9135.795 |

$$\begin{pmatrix} 0 & 0 & 0 & \frac{\beta_L F_L L^* K}{(m_L M^* + L^*)(d_D M^* + dK)} \\ 0 & 0 & 0 & 0 \\ 0 & 0 & 0 & 0 \\ \frac{\beta_M F_N M^* r_2^2}{(\mu_N (m_N M^* + N^*) + F_N M^*)(\mu_L + r_2)^2} & \frac{\beta_M F_N M^* r_2}{(\mu_N (m_N M^* + N^*) + F_N M^*)(\mu_L + r_2)} & \frac{\beta_M F_N M^*}{\mu_N (m_N M^* + N^*) + F_N M^*} & 0 \end{pmatrix}$$

and $\mathcal{R}_0 = \rho(FV^{-1})$ is the square root of the expression in (20) for $n = 2$. The case $n = 2$ can be easily generalized to $n$ larval stages by increasing the upper left $3 \times 2$ matrices in $F$ and $V$ to $(n+1) \times n$ to account for the $n$ stages of $L_1^I$ through $L_n^I$. Thus, for $n$ latent stages, $F$ and $V$ will have dimension $(n + 2) \times (n + 2)$.

Only four disease-free values are required to calculate $\mathcal{R}_0$, $(L^*, N^*, A^*, M^*) = (L, N^S, A, M^S)$. They can be found by setting all of the infected variables in the differential equations equal to zero. For the autonomous case, they can be calculated using the software Maple. The values for the disease-free equilibria for the autonomous ODE and DDE models are found in Table 5. The periodic disease-free solutions can be calculated numerically using MATLAB. See the disease-free periodic solution for the nonautonomous ODE model with $n = 100$ latent stages in Fig. 13.

To ensure that the next generation matrix technique for the autonomous ODE with constant parameters can be applied, several assumptions must be verified (van den Driessche and Watmough 2002; Wang and Zhao 2008). The five conditions (A1)–(A5) are straightforward to verify for the autonomous ODE (e.g., (A5) is the stability of the DFE) (van den Driessche and Watmough 2002). For the nonautonomous ODE with periodic coefficients, there are seven conditions (A1)–(A7). The first five are apparent (Wang and Zhao 2008). Conditions (A6) and (A7) require showing that for the system linearized about the disease-free solution (Fig. 13, $n = 100$ latent stages), $dX/dt = M(t)X$, $X(0) = I_d$ and $dY/dt = -VY$, $Y(0) = I_d$ are stable ($I_d$ is an identity matrix). That is, the fundamental matrices, $\Phi_M(\omega)$ and $\Phi_{-V}(\omega)$, must satisfy $\rho(\Phi_M(\omega)) < 1$ and $\rho(\Phi_{-V}(\omega)) < 1$ ($\omega = 360$). The spectral radii were calculated numerically and found to satisfy the required conditions, $\rho(\Phi_M(\omega)) < 0.39$ and $\rho(\Phi_{-V}(\omega)) < 0.2$ for latent stages $n = 2$, 10 and 100.

## Appendix D: Nonautonomous ODE with $n = 2$ and 10 Latent Stages

Figure 14 is a graph of the ODE solutions for $n = 2$ and 10 latent stages. These graphs can be compared with the ODE solution for $n = 100$ in Fig. 5.

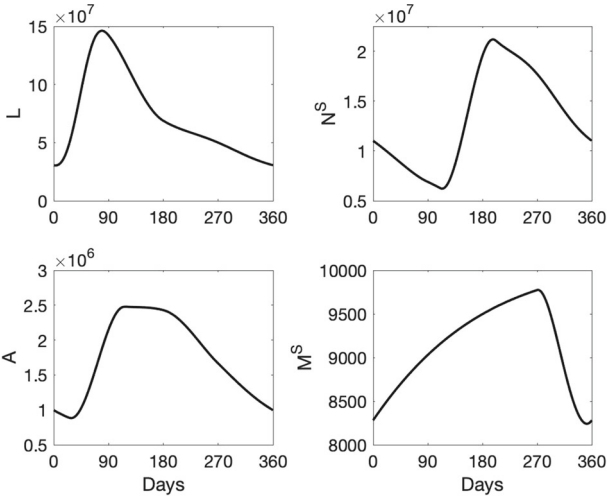


**Fig. 13** Autonomous ODE disease-free periodic solution for $n = 100$ latent stages

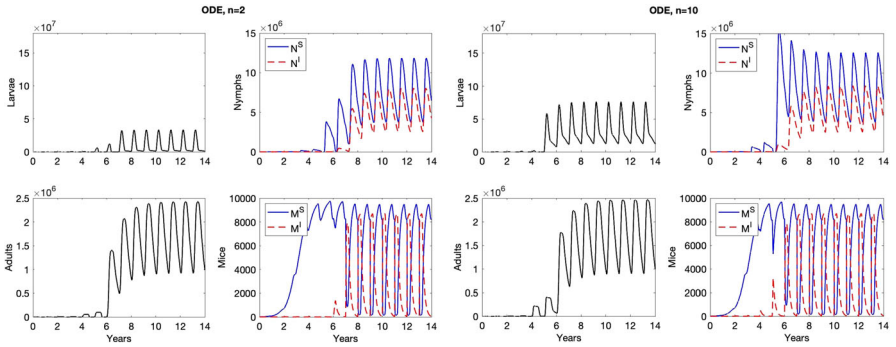


**Fig. 14** Nonautonomous ODE solutions with $n = 2$ or 10 latent stages. Baseline parameters are given in Table 1 and initial conditions are $L(0) = 1000$, $N(0) = 100$, $A(0) = 20$, $M(0) = 10$, $M^I(0) = 2$, with all other initial conditions set to zero. Plots of larvae and adults over time are the stages $L$ and $A$ (Color figure online)

## References

Abramson G, Kenkre V (2002) Mathematical modeling of refugia in the spread of the hantavirus. In: Proceeding of United Science and Technology for Reducing Biological Threats and Countering Terrorism Conference (BTR), vol 64

Allan BF, Keesing F, Ostfeld RS (2003) Effect of forest fragmentation on Lyme disease risk. Conserv Biol 17(1):267–272

Allen LJS, van den Driessche P (2013) Relations between deterministic and stochastic thresholds for disease extinction in continuous-and discrete-time infectious disease models. Math Biosci 243(1):99–108

Allen LJS, Lahodny GE Jr (2012) Extinction thresholds in deterministic and stochastic epidemic models. J Biol Dyn 6(2):590–611

Apanaskevich DA, Oliver JH (2013) Life cycles and natural history of ticks. In: Sonenshine DE, Roe RM (eds) Biology of ticks, vol 1. Oxford University Press, Oxford, pp 59–73

Bacaër N, Ait Dads EH (2014) On the probability of extinction in a periodic environment. J Math Biol 68(3):533–548
Bai F, Huff KES, Allen LJS (2019) The effect of delay in viral production in within-host models during early infection. J Biol Dyn 13(sup1):47–73
Becker DJ, Han BA (2021) The macroecology and evolution of avian competence for Borrelia burgdorferi. Glob Ecol Biogeogr 30(3):710–724
Brunner JL, Ostfeld RS (2008) Multiple causes of variable tick burdens on small-mammal hosts. Ecology 89(8):2259–2272
Caraco T, Gardner G, Maniatty W, Deelman E, Szymanski BK (1998) Lyme disease: self-regulation and pathogen invasion. J Theor Biol 193(4):561–575
Caraco T, Glavanakov S, Chen G, Flaherty JE, Ohsumi TK, Szymanski BK (2002) Stage-structured infection transmission and a spatial epidemic: a model for Lyme disease. Am Nat 160(3):348–359
Carrera-Pineyro D, Hanes H, Litzler A, McCormack A, Velazquez-Molina J, Mubayi A, Ríos-Soto K, Kribs C (2020) Cost analysis of vaccination in tick-mouse transmission of Lyme disease. J Theor Biol 494:110245
Centers for Disease Control and Prevention (CDC) (2020) How ticks spread disease. https://www.cdc.gov/ticks/life_cycle_and_hosts.html. Accessed 23 Jan 2023
Centers for Disease Control and Prevention (CDC) (2021) Ticknet. https://www.cdc.gov/ticknet/index.html. Accessed 03 Feb 2023
Centers for Disease Control and Prevention (CDC) (2023) White-footed mouse. https://www2.illinois.gov/dnr/education/Pages/WAWMWhitefootedMouse.aspx. Accessed 22 Feb 2023
Chen D, Wong H, Belanger P, Moore K, Peterson M, Cunningham J (2015) Analyzing the correlation between deer habitat and the component of the risk for Lyme disease in Eastern Ontario, Canada: a GIS-based approach. ISPRS Int J Geo Inf 4(1):105–123
Chitnis N, Hyman JM, Cushing JM (2008) Determining important parameters in the spread of malaria through the sensitivity analysis of a mathematical model. Bull Math Biol 70(5):1272–1296
Cobbold CA, Teng J, Muldowney JS (2015) The influence of host competition and predation on tick densities and management implications. Thyroid Res 8(3):349–368
Diekmann O, Heesterbeek JAP, Metz JA (1990) On the definition and the computation of the basic reproduction ratio *R*_0 in models for infectious diseases in heterogeneous populations. J Math Biol 28(4):365–382
Eisen RJ, Eisen L, Ogden NH, Beard CB (2016) Linkages of weather and climate with *Ixodes scapularis* and *Ixodes pacificus* (Acari: Ixodidae), enzootic transmission of *Borrelia burgdorferi*, and Lyme disease in North America. J Med Entomol 53(2):250–261
Fan G, Thieme HR, Zhu H (2015) Delay differential systems for tick population dynamics. J Math Biol 71(5):1017–1048
Fulk A, Huang W, Agusto F (2022) Exploring the effects of prescribed fire on tick spread and propagation in a spatial setting. Comput Math Methods Med 2022:5031806. https://doi.org/10.1155/2022/5031806
Gaff H, Eisen RJ, Eisen L, Nadolny R, Bjork J, Monaghan AJ (2020) LYMESIM 2.0: an updated simulation of blacklegged tick (Acari: Ixodidae) population dynamics and enzootic transmission of Borrelia burgdorferi (Spirochaetales: Spirochaetaceae). J Med Entomol 57(3):715–727
Gaff HD, Gross LJ (2007) Modeling tick-borne disease: a metapopulation model. Bull Math Biol 69(1):265–288
Gillespie DT (1977) Exact stochastic simulation of coupled chemical reactions. J Phys Chem 81(25):2340–2361
Guo E, Agusto FB (2022) Baptism of fire: modeling the effects of prescribed fire on Lyme disease. Can J Infect Dis Med Microbiol 2022:5300887. https://doi.org/10.1155/2022/5300887
Heffernan JM, Smith RJ, Wahl LM (2005) Perspectives on the basic reproductive ratio. J R Soc Interface 2(4):281–293
Heffernan JM, Lou Y, Wu J (2014) Range expansion of *Ixodes scapularis* ticks and of *Borrelia burgdorferi* by migratory birds. Discret Contin Dyn Syst-B 19(10):3147
Hesselton WT, Hesselton RM (1982) White-tailed deer. In: Chapman JA, Feldhamer GA (eds) Wild mammals of North America: biology, management, and economics. The Johns Hopkins University Press, Baltimore, pp 878–901
Husar K, Pittman D, Rajala J (2021) Tick-mouse models for Lyme disease with seasonal variation in birth, death, and tick feeding. Texas Tech University Summer REU Report https://www.math.ttu.edu/undergraduate/reu2021/

Jones CG, Ostfeld RS, Richard MP, Schauber EM, Wolff JO (1998) Chain reactions linking acorns to gypsy moth outbreaks and Lyme disease risk. Science 279(5353):1023–1026
Keesing F, Brunner J, Duerr S, Killilea M, LoGiudice K, Schmidt K, Vuong H, Ostfeld R (2009) Hosts as ecological traps for the vector of Lyme disease. Proc R Soc B Biol Sci 276(1675):3911–3919
Kugeler KJ, Schwartz AM, Delorey MJ, Mead PS, Hinckley AF (2021) Estimating the frequency of Lyme disease diagnoses, United States, 2010–2018. Emerg Infect Dis 27(2):616
Lindsay LR, Barker IK, Surgeoner GA, McEwen SA, Gillespie TJ, Robinson JT (1995) Survival and development of *Ixodes scapularis* (Acari: Ixodidae) under various climatic conditions in Ontario, Canada. J Med Entomol 32(2):143–152
Lloyd AL (2001) Realistic distributions of infectious periods in epidemic models: changing patterns of persistence and dynamics. Theor Popul Biol 60(1):59–71
LoGiudice K, Ostfeld RS, Schmidt KA, Keesing F (2003) The ecology of infectious disease: effects of host diversity and community composition on Lyme disease risk. Proc Natl Acad Sci 100(2):567–571
Lou Y, Wu J (2014) Tick seeking assumptions and their implications for Lyme disease predictions. Ecol Complex 17:99–106
Lou Y, Wu J (2017) Modeling Lyme disease transmission. Infect Dis Model 2(2):229–243
Lou Y, Wu J, Wu X (2014) Impact of biodiversity and seasonality on Lyme-pathogen transmission. Theor Biol Med Model 11(1):1–25
Maliyoni M, Chirove F, Gaff HD, Govinder KS (2017) A stochastic tick-borne disease model: exploring the probability of pathogen persistence. Bull Math Biol 79(9):1999–2021
Martcheva M (2015) An introduction to mathematical epidemiology, vol 61. Springer, New York
Mead P (2022) Epidemiology of lyme disease. Infect Dis Clin North Am 36(3):495–521
Miller KV, Muller LI, Demarais S (2003) White-tailed deer (*Odocoileus virginianus*). In: Feldhamer GA, Thompson BC, Chapman JA (eds) Wild mammals of North America: biology, management, and conservation, 2nd edn. Johns Hopkins University Press, Baltimore, pp 906–930
Mount G, Haile D, Daniels E (1997) Simulation of blacklegged tick (Acari: Ixodidae) population dynamics and transmission of *Borrelia burgdorferi*. J Med Entomol 34(4):461–484
Nah K, Wu J (2021) Long-term transmission dynamics of tick-borne diseases involving seasonal variation and co-feeding transmission. J Biol Dyn 15(1):269–286
Nipa KF, Jang SRJ, Allen LJS (2021) The effect of demographic and environmental variability on disease outbreak for a dengue model with a seasonally varying vector population. Math Biosci 331:108516
Novella IS, Quer J, Domingo E, Holland JJ (1999) Exponential fitness gains of RNA virus populations are limited by bottleneck effects. J Virol 73(2):1668–1671
Ogden N, Lindsay L, Beauchamp G, Charron D, Maarouf A, O'Callaghan C, Waltner-Toews D, Barker I (2004) Investigation of relationships between temperature and developmental rates of tick *Ixodes scapularis* (Acari: Ixodidae) in the laboratory and field. J Med Entomol 41(4):622–633
Ogden N, Bigras-Poulin M, O'callaghan C, Barker I, Lindsay L, Maarouf A, Smoyer-Tomic K, Waltner-Toews D, Charron D (2005) A dynamic population model to investigate effects of climate on geographic range and seasonality of the tick *Ixodes scapularis*. Int J Parasitol 35(4):375–389
Ogden NH, Bigras-Poulin M, O'Callaghan CJ, Barker IK, Kurtenbach K, Lindsay LR, Charron DF (2007) Vector seasonality, host infection dynamics and fitness of pathogens transmitted by the tick *Ixodes scapularis*. Parasitology 134(2):209–227
Ogden NH, Lindsay LR, Hanincová K, Barker IK, Bigras-Poulin M, Charron DF, Heagy A, Francis CM, O'Callaghan CJ, Schwartz I et al (2008) Role of migratory birds in introduction and range expansion of *Ixodes scapularis* ticks and of *Borrelia burgdorferi* and *Anaplasma phagocytophilum* in Canada. Appl Environ Microbiol 74(6):1780–1790
Ostfeld RS, Jones CG, Wolff JO (1996) Of mice and mast. Bioscience 46(5):323–330
Ostfeld RS, Canham CD, Oggenfuss K, Winchcombe RJ, Keesing F (2006) Climate, deer, rodents, and acorns as determinants of variation in Lyme-disease risk. PLoS Biol 4(6):e145
Ostfeld RS, Levi T, Keesing F, Oggenfuss K, Canham CD (2018) Tick-borne disease risk in a forest food web. Ecology 99(7):1562–1573
Pearson P, Rich C, Feehan MJ, Ditchkoff SS, Rich SM (2023) White-tailed deer serum kills the Lyme disease spirochete, *Borrelia burgdorferi*. Vector-Borne Zoonotic Dis 23(5):303–305
Pittman DC (2022) Models for fluctuating mice populations using demographic, seasonal, infection, and ecological changes with periodic stochastic methods. Bachelor's honors thesis, Washington State University, Pullman

Public Health Agency of Canada (PHAC) (2023) Lyme disease surveillance report: Annual edition, 2020. https://www.canada.ca/en/public-health/services/publications/diseases-conditions/lyme-disease-surveillance-canada-annual-edition-2020.html. Accessed 01 Oct 2023

Rollend L, Fish D, Childs JE (2013) Transovarial transmission of Borrelia spirochetes by *Ixodes scapularis*: a summary of the literature and recent observations. Ticks Tick-Borne Dis 4(1–2):46–51

Sauvage F, Langlais M, Yoccoz NG, Pontier D (2003) Modelling hantavirus in fluctuating populations of bank voles: the role of indirect transmission on virus persistence. J Anim Ecol 72(1):1–13

Schwartz AM, Hinckley AF, Mead PS, Hook SA, Kugeler KJ (2017) Surveillance for Lyme disease-United States, 2008–2015. MMWR Surveill Summ 66(22):1

Shakiba N, Edholm CJ, Emerenini BO, Murillo AL, Peace A, Saucedo O, Wang X, Allen LJS (2021) Effects of environmental variability on superspreading transmission events in stochastic epidemic models. Infect Dis Model 6:560–583

States S, Huang C, Davis S, Tufts D, Diuk-Wasser M (2017) Co-feeding transmission facilitates strain coexistence in Borrelia burgdorferi, the Lyme disease agent. Epidemics 19:33–42

Tilly K, Rosa PA, Stewart PE (2008) Biology of infection with *Borrelia burgdorferi*. Infect Dis Clin North Am 22(2):217–234

van den Driessche P (2017) Reproduction numbers of infectious disease models. Infect Dis Model 2(3):288–303

van den Driessche P, Watmough J (2002) Reproduction numbers and sub-threshold endemic equilibria for compartmental models of disease transmission. Math Biosci 180(1):29–48

Vessey SH (1987) Long-term population trends in white-footed mice and the impact of supplemental food and shelter. Am Zool 27(3):879–890

Voordouw MJ (2015) Co-feeding transmission in Lyme disease pathogens. Parasitology 142(2):290–302

Wang W, Zhao XQ (2008) Threshold dynamics for compartmental epidemic models in periodic environments. J Dyn Differ Equ 20(3):699–717

Wang X, Zhao XQ (2017) Dynamics of a time-delayed Lyme disease model with seasonality. SIAM J Appl Dyn Syst 16(2):853–881

Wesley CL, Allen LJS (2009) The basic reproduction number in epidemic models with periodic demographics. J Biol Dyn 3(2–3):116–129

Wu J, Zhang X (2020) Transmission dynamics of tick-borne diseases with co-feeding, developmental and behavioural diapause. Springer Nature, Switzerland

Wu X, Röst G, Zou X (2016) Impact of spring bird migration on the range expansion of *Ixodes scapularis* tick population. Bull Math Biol 78:138–168

Zhang X, Wu J (2019) Critical diapause portion for oscillations: parametric trigonometric functions and their applications for Hopf bifurcation analyses. Math Methods Appl Sci 42(5):1363–1376

Zhang X, Sun B, Lou Y (2021) Dynamics of a periodic tick-borne disease model with co-feeding and multiple patches. J Math Biol 82(4):1–27

Zhang Y, Zhao XQ (2013) A reaction-diffusion Lyme disease model with seasonality. SIAM J Appl Math 73(6):2077–2099